1985

Continuum flow sampling mass spectrometer for elemental analysis with an inductively coupled plasma ion source

José Antonio Olivares
Iowa State University

Olivares, Jose Antonio

CONTINUUM FLOW SAMPLING MASS SPECTROMETER FOR ELEMENTAL ANALYSIS WITH AN INDUCTIVELY COUPLED PLASMA ION SOURCE

Iowa State University PH.D. 1985

Continuum flow sampling mass spectrometer for elemental analysis with an inductively coupled plasma ion source

by

José Antonio Olivares

A Dissertation Submitted to the
Graduate Faculty in Partial Fulfillment of the
Requirements for the Degree of
DOCTOR OF PHILOSOPHY

Department: Chemistry
Major: Analytical Chemistry

Approved:

Signature was redacted for privacy.

In Charge of Major Work

Signature was redacted for privacy.

For the Major Department

Signature was redacted for privacy.

For the Graduate College

Iowa State University
Ames, Iowa

1985

TABLE OF CONTENTS

DEDICATION

To Phiyen, Cecilia, Gabriel and Javier

Your patience and support have made

these the best years of my life.

PREFACE

Since the development of inductively coupled plasma-mass spectrometry (ICP-MS) in 1980 by R. S. Houk under the direction of Professors Fassel and Svec at Iowa State University, the ICP-mass spectrometric technique has seen growth in the development of the instrumentation and also in the acceptance by the scientific community as a viable technique for elemental analysis. Much of the development in the instrumentation has been in the construction of the mass spectrometer interface. But the emphasis on the analytical capabilities of ICP-MS has overshadowed this development and the understanding of the limitations that the instrumentation imposes on the observed analytical signals. It is the overall purpose of this thesis to provide a basic understanding of the construction and performance of the ICP-mass spectrometer interface, and the physical and chemical limitations that have been observed with this instrument.

The format of this thesis is divided into three sections. Each section stands alone as a complete manuscript with Figures, Tables and Literature Cited all numbered in consecutive order within each section. The first section deals with the sampling of ions from an ICP with a supersonic nozzle and skimmer. The construction of such a system and its behavior are compared to similar systems for ion sampling from other plasmas and flames. A design for an off-axis detector for background suppression and the dependence of spectral interferences from the for-

mation of metal oxides and doubly charged ions on ICP operating parameters are also discussed.

The signal observed from a mass spectrometer is often a sensitive function of the characteristics of the ions made at the ion source. In the second section of this thesis, a method is described for the approximate measurement of the ion energy distribution in an ICP-mass spectrometer. The average ion kinetic energy, kinetic energy spread, and maximum kinetic energy are evaluated from a plot of ion signal as a function of retarding voltage applied to the quadrupole mass analyzer. Using this technique the effects of plasma operating parameters on ion signals and energies are described.

The ICP has a relatively high tolerance for solutions with high salt concentrations without adverse effects on the observed analytical signal of minor constituents. In the last section of this thesis the interference on the ionization of cobalt by five salts, NaCl, $MgCl_2$, NH_4I, NH_4Br, and NH_4Cl, in an ICP is first considered theoretically and subsequently the theoretical trends are established by ICP-MS.

An attempt has been made to keep each section independent with as little redundancy as possible throughout the sections. Due to the overlap of the subject matter such redundancies could not be avoided in some cases.

SECTION I.

ION SAMPLING FOR INDUCTIVELY COUPLED PLASMA MASS SPECTROMETRY

INTRODUCTION

The first analytical mass spectrometer for ion sampling from an inductively coupled plasma (1) used a stagnant layer type sampling interface (Figure 1), subsequently referred to as boundary layer sampling. In this technique ions and neutrals were extracted from an aerodynamic boundary layer that formed in front of the sampling cone. The difficulties associated with this type of sampling were quickly realized by the observation of metal oxide and metal hydroxide ions, deposition of salts on the orifice and short orifice lifetime.

Supersonic nozzle beam sources for dynamic sampling of ions and neutrals from flames and plasmas have been in use since the pioneering work of Kantrowitz and Grey (2) in 1951. The version of this technique used in inductively coupled plasma mass spectrometry (ICP-MS) employs a large sampling orifice, through which the source gas flows under continuum conditions into an evacuated expansion stage. Part of the supersonic beam that forms in the expansion stage is then skimmed by a conical skimmer and introduced into a second vacuum stage. Gray and Date (3) and Douglas et al. (4) applied supersonic nozzle interfaces to ICP-mass spectrometers finding overall improved performance in ion sampling. Yet, little has been described in the literature on the adaptation of supersonic nozzles to the ICP, with most of the published work emphasizing the analytical capabilities of ICP-MS.

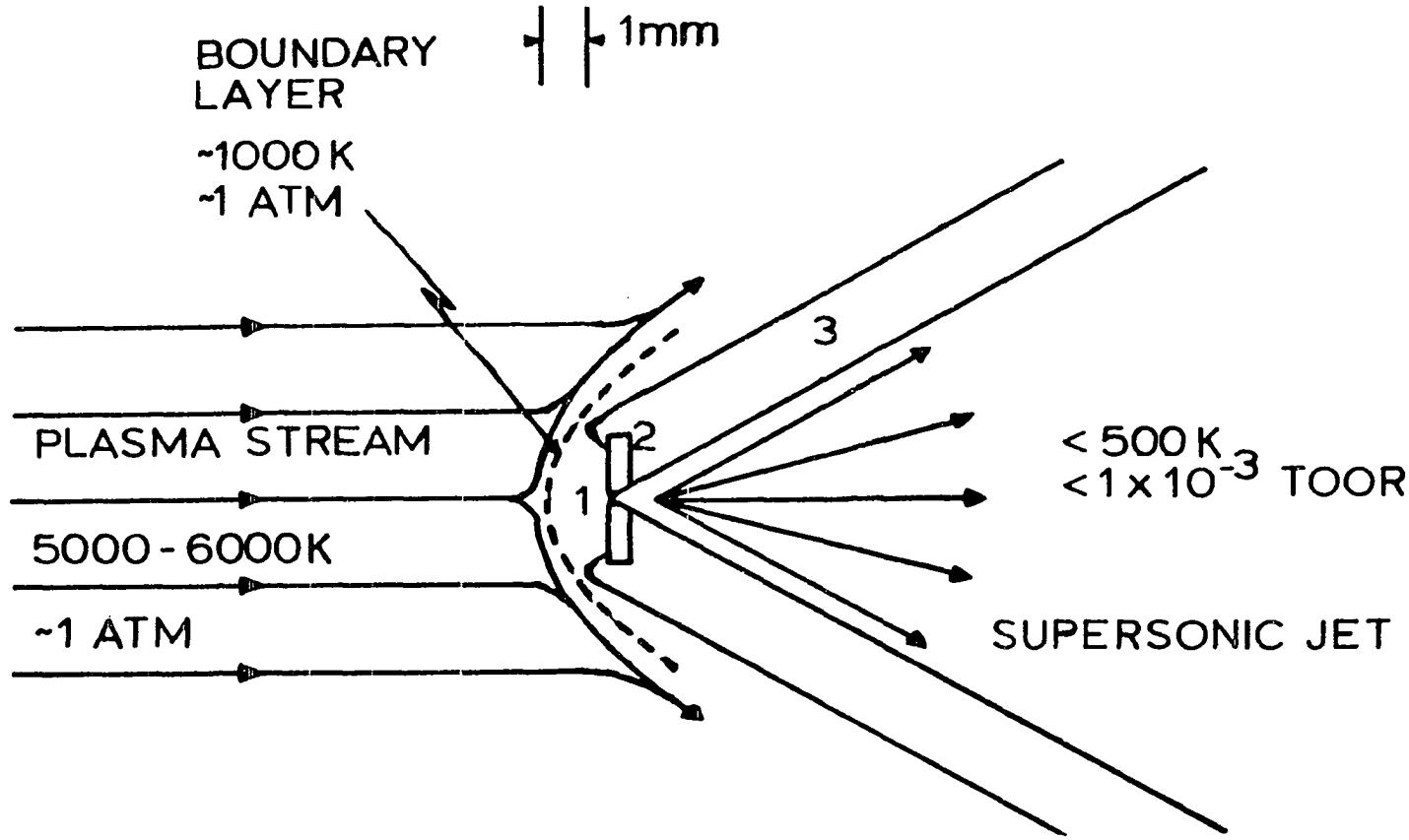

Figure 1. Diagram of boundary layer sampling interface for ICP-MS: (1) sampling orifice (50 µm diameter); (2) molybdenum disk containing orifice; (3) copper cone with spun copper seal to retain molybdenum disk

Ion focusing, detection and background suppression is another area of research in ICP-MS where common information is lacking. Most instruments employ a Bessel box (5,6) or a modification of this for ion focusing in the transition flow region behind the skimmer. This device consists of an arrangement of three lenses, a cylinder and two rings on each end. The cylinder contains, at its center, a round plate with a diameter nearly equal to or less than the inside diameter of the end rings. The arrangement, when used with appropriate voltages applied to the lenses, provides an effective energy analyzer. The Bessel box was originally implemented for ICP-MS partly because it was believed that ion energy analysis was necessary. But, when this was found not to be the case (3) this lens arrangement remained in use because the center plate provides an effective shield for blocking ICP photons from the detector. The central axis of a Bessel box is physically blocked so that the ion transmission efficiency of this device is relatively low compared to an open ion lens focusing system. Therefore, our research has emphasized producing a detector arrangement which minimizes the detection of background photons and can collect a major portion of the mass analyzed ion beam, using conventional electrostatic ion focusing in the transition flow region.

In this paper, we describe in detail the construction and performance characteristics of a supersonic nozzle for ICP-MS with ion sampling in the continuum flow regime, the performance of an off-axis

detector arrangement for photon background suppression, and the overall analytical performance of this instrument.

APPARATUS

A schematic diagram of the ICP-mass spectrometer used in this work is shown in Figure 2, with a brief description of each component given in the caption. Most instrumental components in this arrangement are described elsewhere (7). A rigorous treatment of particular components of interest follows. Unless otherwise stated, the general ICP operating conditions are given in Table I.

Computer Control Interface

Computer control of the mass spectrometer is achieved through a 16 bit digital to analog converter (DAC) (T), with an output range of 0 - 10 V dc. The interface was assembled at the Ames Laboratory and consists primarily of a DAC 1136 (Analog Devices, Norwood, MA). Control of the DAC is achieved by a DRV11 parallel line unit (MDB Systems Inc., Orange, CA) on a PDP-11/73 microcomputer (S) (Digital Equipment Corp., Maynard, MA).

Data acquisition from the TTL compatible output of the amplifier-discriminator (Q) (Model 1762, Photochemical Research Associates, Oak Ridge, TN) is achieved with a pulse counting board (R) (Model 1604-OPI-2, ADAC Corp., Woburn, MA). The two 16 bit input channels on this board were daisy chained to make one 32 bit input channel.

A programmable real-time clock (MLSI-KW11P, MDB Systems Inc.) was used for synchronization of the quadrupole control and data acquisition

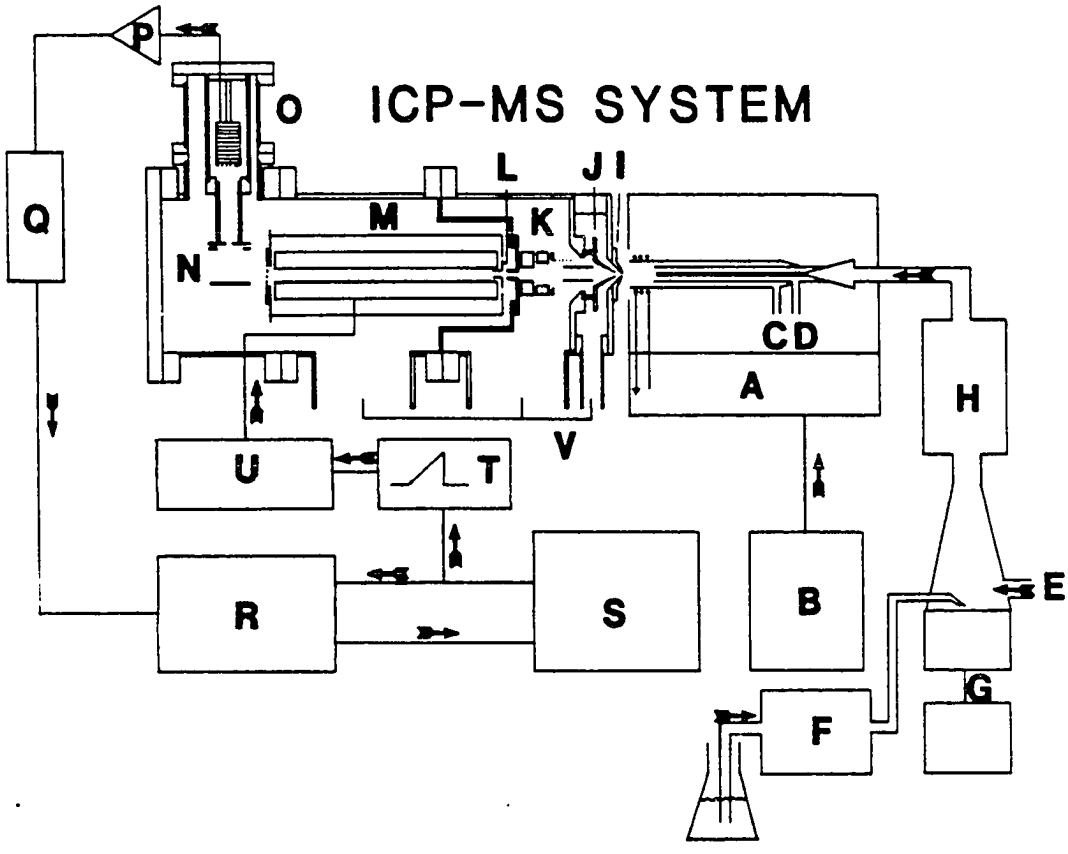

Figure 2. Experimental apparatus: (A) ICP, torch and impedance matching network; (B) 27.12 MHz RF generator; (C) inlet for argon outer gas; (D) inlet for argon auxiliary gas; (E) inlet for argon aerosol gas; (F) peristaltic pump for solution uptake; (G) ultrasonic nebulizer and power supply; (H) desolvation apparatus; (I) nickel sampling cone; (J) stainless steel skimmer; (K) ion focusing lenses; (L) ELFS lens; (M) quadrupole mass analyzer; (N) detector assembly, repeller plate and focusing plates and cylinder; (O) electron multiplier; (P) pulse counting preamplifier; (Q) amplifier-discriminator; (R) counting-computer interface; (S) computer; (T) 16 bit DAC; (U) quadrupole control electronics; (V) pumps

Table I. Experimental Parameters

Plasma outer argon gas flow rate	17 l/min
Auxiliary argon gas flow rate	0.5 l/min
Aerosol argon gas flow rate	0.43 l/min
Plasma forward power	1.1 kW
Solution uptake to nebulizer	1.8 ml/min
Sampling position	7 mm above load coil Sampler centered on axial channel

system. A NAND gate (74LS00 chip) between the output of the amplifier-discriminator and the input of the counting board, controlled by the high/low done bit of the clock, assured that counting was synchronous with the clock and independent of the computer interrupt response time. Multi-purpose programs for mass spectrum scanning and multiple ion monitoring were written in FORTRAN with real time graphics display in MACRO-11 assembly language.

Ion Sampling Interface

A scale drawing of the ICP-mass spectrometer sampling interface is shown in Figure 3. The nozzle or sampling cone (A) is made from nickel with 90° and 120° internal and external angles, respectively. A 0.53 mm diameter orifice with a length of approximately 0.25 mm is drilled in the tip of this cone. The skimmer (B) is made from stainless steel with 50° and 60° internal and external angles, respectively. The skimmer orifice is sharp and has a 1.40 mm diameter. The distance between the nozzle and the skimmer orifice was varied by changing the thickness of the teflon spacer (C) between the skimmer base and the vacuum chamber. Unless otherwise indicated, the skimmer and sampler were grounded. The pressure in the first expansion chamber was measured by a Convectron gauge (Model no. 151, Granville Phillips, Boulder, CO).

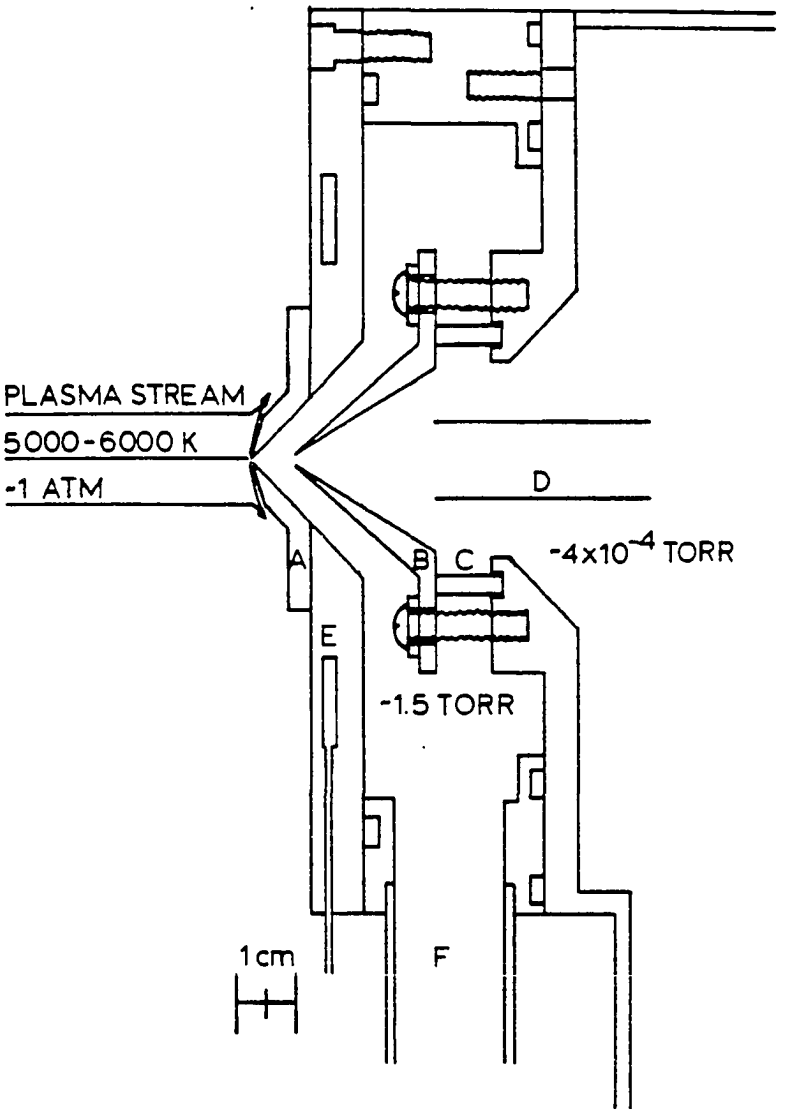

Figure 3. Scale drawing of continuum sampling interface for ICP-MS: (A) nozzle; (B) skimmer; (C) teflon spacer; (D) extraction ion lens; (E) cooling water

Detector Assembly

The detector arrangement is shown in Figure 2N. Either focused mesh (Model no. MM2-1SG, Johnston Laboratories, Inc., Cockeysville, MD) or a Channeltron (Model no. 4830, Galileo Electro-Optics Co., Sturbridge, MA) multiplier was used with similar performance. The cylinder between the mass analyzer and the multiplier is 6.6 cm long by 2.5 cm in diameter and is used to focus ions into the electron multiplier. This cylinder must be kept at a higher negative potential than the electron multiplier, otherwise the multiplier appears to suffer a loss in gain and signal. Presumably this is because electrons formed at the cathode are lost to the cylinder rather than travel down the multiplier tube. The plate directly below the mesh exit lens from the mass analyzer is operated at a positive potential (~ +200 V dc) in order to repel ions into the focus cylinder. Computer simulation of this detector arrangement, with SIMION (8,9), shows 30% efficiency in the detection of 10 eV ions leaving the quadrupole exit grid in parallel paths to the quadrupole axis and with uniform radial distribution. Peripheral ions are readily lost.

RESULTS AND DISCUSSION

Sampling Interface Theory and Performance

In order to understand the performance of the supersonic nozzle sampling interface described above, it is instructive to compare experimental results with the expected behavior of such systems. For viscous flow, the gas flow through the nozzle is given by Eq. 1 (10)

$$U_0 = \frac{\Pi f(\gamma) N_A D_0^2 P_0}{4(MRT_0)^{1/2}} \qquad (1)$$

where: $f(\gamma) = \gamma^{1/2}\left[\frac{2}{\gamma+1}\right]^{(\gamma+1)/2(\gamma-1)}$

U_0 ≡ flow through orifice (molecules/s)

N_A ≡ Avogadro's number

D_0 ≡ orifice diameter (= 0.00053 m)

P_0 ≡ ICP pressure (= 1 atm = 1.0×10^5 kg m^{-1} s^{-2})

M ≡ mean molecular weight of the gas (argon for ICP)

R ≡ gas constant

T_0 ≡ gas temperature of ICP (= 5000 K)

γ ≡ specific heat ratio, $\left(\frac{C_P}{C_V}\right)$, of argon (= 1.67).

Equation 2 (11) relates Eq. 1 to the gas flow through the skimmer (U_S).

$$U_S = U_0 f(\gamma) \left(\frac{D_S}{X_S}\right)^2 \qquad (2)$$

In Eq. (2): $D_S \equiv$ skimmer diameter (= 1.40 mm)

$X_S \equiv$ skimmer to nozzle distance.

The theoretical flow of gas molecules through the skimmer is plotted in Figure 4a for different skimmer to nozzle distances. The detected ion signal from the ICP of a 10 mg L^{-1} Co solution, Figure 4b, resembles the theoretical curve when X_S is greater than 0.75 cm. There is a deviation from the theoretical curve at large and small skimmer to nozzle distances. Such deviations have been observed by other workers (12) for nonionized molecular beams. The shape of Figure 4b can be rationalized from an understanding of the shock wave formation down stream from the orifice, i.e., the Mach disk. The Mach disk phenomenon is depicted schematically in Figure 5a and results from interaction of the expanding jet with background gas in the vacuum chamber. Extensive scattering of sampled particles occurs at the Mach disk or downstream from it (13). Ashkenas and Sherman (14) have shown that the Mach disk forms at a distance X_M from the orifice given by Eq. 3:

$$X_M = 0.67\ D_0 \left(\frac{P_0}{P_1}\right)^{1/2} \qquad (3)$$

where P_1 is the background pressure in the expansion chamber (1.5 torr). For our work X_M = 0.80 cm, which corresponds closely to the nozzle-

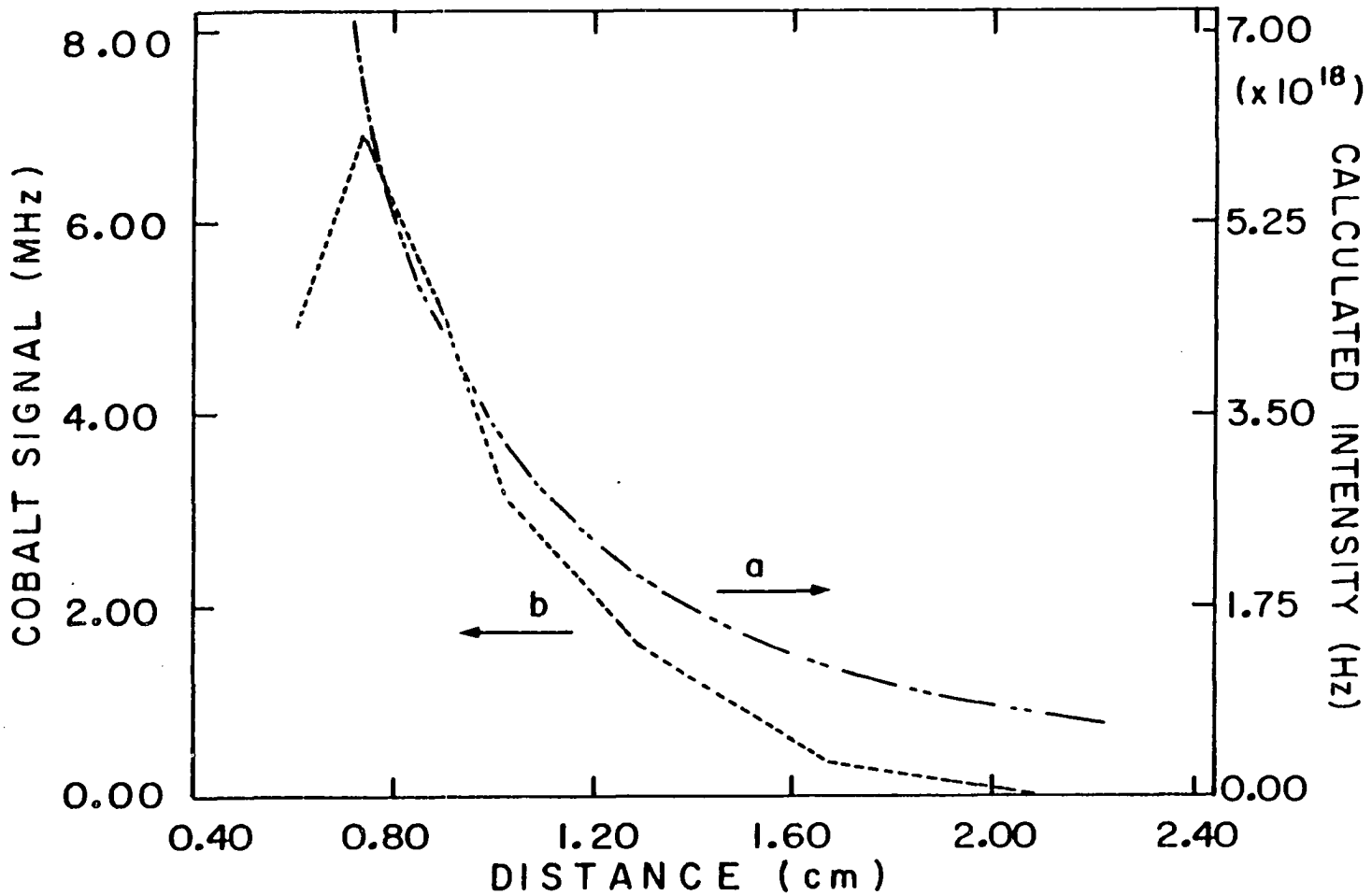

Figure 4. Flow from ICP source through a 1.40 mm diameter skimmer versus nozzle-to-skimmer distance: a) theoretical gas flow; b) experimentally measured Co^+ signal

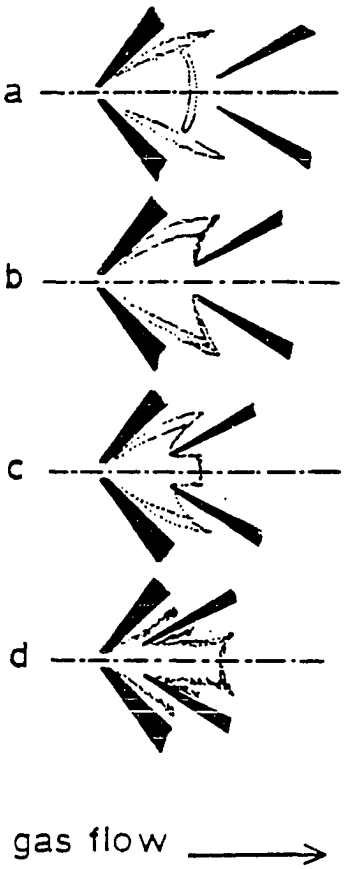

Figure 5. Schematic picture of supersonic beam formation through adiabatic expansion at the sampling cone and skimmer cone interaction at different intercone distances (reproduced with permission from the editor from Ref. 13)

skimmer distance at which maximum ion intensity is measured. Finally, we conclude the following using Figure 5 as a schematic representation of the Mach disk formation (13). For $X_S > X_M$, the shock wave forms in front of the skimmer and flow of ions through the skimmer is dominated by effusion of the ions that have been scattered by the shock (Figure 5a). For $X_S \approx X_M$, there is little ion scattering between the nozzle and ion collection lens behind the skimmer, and therefore maximum ion beam intensity is achieved (Figure 5b). For $X_S < X_M$, a shock wave forms inside or downstream from the skimmer (Figure 5c and d), in front of or at the collection ion lens (Figure 3D), which scatters ions, making ion collection and focusing difficult.

It is further understood from molecular beam experiments that maximum beam intensity is achieved at a Knudsen number (Kn) of 1 at the skimmer, where the Knudsen number is given by (15):

$$Kn = \frac{\lambda}{D_S} = \frac{(16/5)\eta}{D_S n \pi \sqrt{2\pi kT/m}} \qquad (4)$$

where: η ≡ viscosity coefficient of argon (= 0.6 mpoise)

n ≡ the number density = P_i/RT

P_i = impact pressure at skimmer orifice

$0.6595\ (X_S/D_0)^{-2} P_0$ (for argon)

m ≡ mean molecular weight of the gas

k ≡ Boltzmann's constant

T ≡ the local gas temperature at the skimmer

D_S ≡ skimmer diameter

λ ≡ mean free path

Although the gas temperature at the skimmer has not been measured for ICP sampling, a reasonable range of 500 - 800 K can be estimated from observations of the thermal temperatures achieved by the base of the skimmer where nylon spacers and soft solder readily melt. From the above information, λ = 0.13 - 0.10 cm and Kn = 0.9 - 0.7, which is close to the recommended (13) skimming Knudsen number for least disturbance of the jet expansion. Note that this is achieved with a relatively low pumping speed in the expansion chamber (~10 L/s) and it is mainly due to the relatively high gas temperature of the plasma from which the gas flow is lower, by a factor of 4, than for atmospheric pressure sources at room temperature.

Therefore, it is emphasized from the above observations, that the ICP-MS ion sampling interface should be designed using the well-known principles of supersonic nozzle design for high intensity neutral beams. This conclusion is not too surprising because the total particle density in the ICP is of the order of 10^{18} cm^{-3}, while the charged particle density is of the order of 10^{14} - 10^{15} cm^{-3} (16). Thus, most of the gas flowing through the nozzle is neutral. Ion-electron recombination probably occurs in the early stages of the expansion to further reduce the fraction of sampled gas that remains ionized. The arguments above indi-

cate that ions are extracted through the nozzle and transmitted through the skimmer primarily by entrainment in a predominantly neutral gas stream. Furthermore, with our present sampling arrangement the sampler and skimmer are held at the same potential (ground). It is feasible to isolate the skimmer electrically by supporting it with insulating bolts so that a separate potential can be applied from an external power supply. In principle, such an arrangement should permit use of the skimmer as an ion lens in addition to its flow collimation function described above. For example, application of a negative potential to the skimmer would be expected to repel electrons and attract positive ions through the skimmer orifice (17). As yet, we have found no consistent advantage to biasing the skimmer electrically because it tends to discharge, drawing considerable current (up to ~ 0.5 A) from the power supply and causing the background and ion energies to increase without yielding appreciably better signals. In future experiments, we intend to seek ion sampling and skimming conditions that permit application of different potentials to the skimmer and sampler without these deleterious effects.

Ion Focusing in the Transition Flow Regime

The electrostatic cylindrical ion lens shown in Figure 2K represents the best working arrangement out of several different configurations attempted. Ion focusing in this region of the mass spectrometer is difficult because of the transition from collision dominated flow to

molecular flow along the beam axis. This transition phenomenon is evident because ions can be detected even if the skimmer and first extraction lens are biased at voltages of up to + 100 V dc. We attribute this observation to collisions in the beam that can scatter ions through a region of relatively high positive potential in the early stages of the expansion. Once the positive ion is scattered into a positive region (e.g., the extraction cylinder, Figure 3D) it acts as if it were formed there and is driven downstream towards the other, negatively biased elements of the ion lens (Figure 2K). With the skimmer grounded and first extraction lens grounded the downstream lenses will cut off analyte ion transmission at voltages $\gtrsim$ +10 V dc. This indicates that the local pressure in the beam has been reduced to the molecular flow regime and scattering collisions are much less common inside these downstream components.

Darcie (18) applied the Boltzmann equation to the case of transition flow of ions in a mostly neutral beam, through a region of constant axial electrical field (i.e., drift tube) and uniform target gas density. It would be interesting to perform similar experimental and theoretical studies for the ion extraction and focusing geometry used in ICP-MS. Furthermore, the high ion currents sampled from the ICP may make it necessary for any successful analytical treatment to consider space charge and discharge effects. These are evident by a lag in the response of the measured ion signal to a change in particular electrostatic lens potentials, and also by an increase in background (presum-

ably due to photon emission) when the skimmer and the first extraction lens (Figure 3D) are set at high positive or negative potentials. The power supply on the first extraction lens draws up to 100 mA of current while sampling ions from the ICP. In fact, in our instrument, a trade off must be made when setting the voltage on these lenses, and optimum performance is found when these are set near or at ground. An upper estimate of the ion current through the sampling orifice can be obtained from Eq. 5 (19), which disregards ion losses to the walls and neutralization processes.

$$i_+ = n_+ e \pi \frac{D_0^2}{4} \left(\frac{RT_0 a}{M}\right)^{1/2} \qquad (5)$$

In Eq. (5): $i_+ \equiv$ ion current through the orifice (A),

$n_+ \equiv$ ion density in the plasma (1×10^{15} cm^{-3}),

$e \equiv$ elementary charge,

and $a = \gamma\left(\frac{2}{\gamma+1}\right)^{(\gamma+1)/(\gamma-1)}$.

With this equation and Eq. (2) for gas flow as a function of nozzle-skimmer distance, one can estimate a current of 0.25 mA at the entrance of a 1.25 cm diameter lens 2.5 cm away from the skimmer. Such ion currents exceed the maximum ion current required for negligible space charge effects (15), which for the extraction lens size used in this work is approximately 1 μA. The severity of space charge effects

in the ion lens will depend upon the efficiency of collision processes that neutralize ions during the extraction. This efficiency is difficult to estimate quantitatively unless the transmission efficiency of the ion lens, mass analyzer, and detector are known accurately.

Analytical Performance

The analyte count rates for elements with ionization energies less than 8 eV are 1 - 5 MHz per mg L^{-1} and are dependent upon various operating parameters for the ICP, ion lens, and mass analyzer. The background is between 1 - 10 kHz, again depending on operating conditions. Figure 6 shows a spectrum recorded for a 1 mg L^{-1} copper solution in 1% nitric acid. The standard deviation of the background in Figure 6 is 100 Hz so the detection limit (2σ) for ^{63}Cu is 0.2 μg L^{-1} . The spectrum shows the high intensity of the background ions at $m/z \leq 41$. The ion peaks due to Ar^+ and ArH^+, at $m/z = 40$ and 41, respectively, appear split because at ion currents greater than 10 MHz the electron multiplier can no longer produce discrete pulses when operating in the ion counting mode (the amplifier-discriminator is rated for ion count rates up to 100 MHz). The peaks at $m/z = 54$ and 56 are presumed to be ArN^+ and ArO^+. In distilled water solution, the ArN^+ peak decreases significantly relative to 1% nitric acid solutions.

Isotope ratios may be measured with a precision of the order of 1% for nearly equal ratios, with the precision getting poorer as the ratio deviates from unity and the solution concentration decreases. Table II

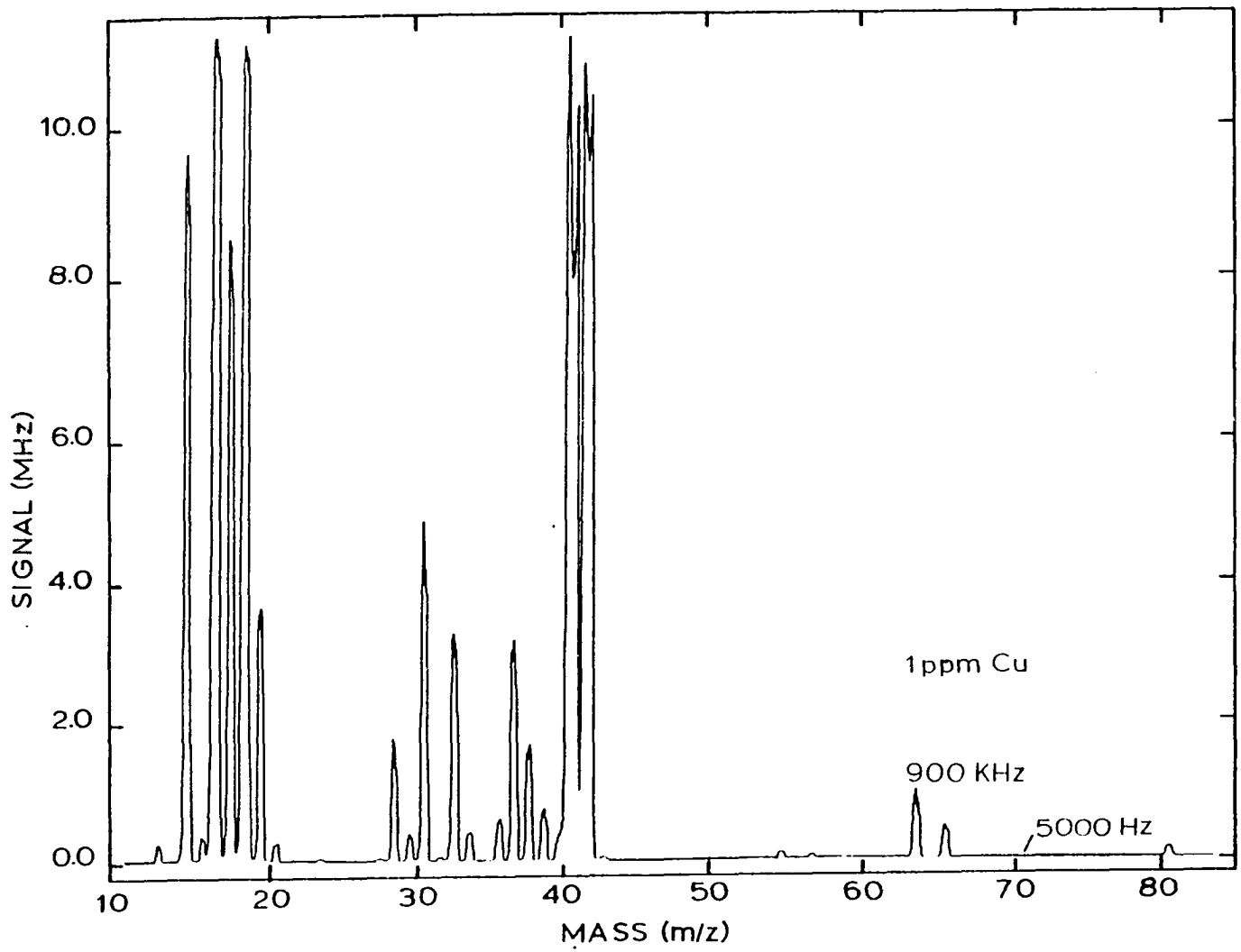

Figure 6. Mass spectrum of a 1 mg L^{-1} Cu solution in 1% HNO_3

Table II. Lead isotope ratios by flow injection analysis with ICP-MS

Sample	Isotopes	# of Injections	Ratio[a]	% RSD	Certification
Fisher	208/207		2.358	0.9	
Standard	208/206	6	1.922	1.0	Natural
	208/204		55.2	5.5	
	208/207		2.250	0.4	2.37055
SRM981	208/206	5	2.074	0.4	2.16810
	208/204		44.2	12	36.7484
	208/207		2.035	0.7	2.14134
SRM982	208/206	5	0.9766	0.2	1.00016
	208/204		43.3	13	36.744
	206/207		14.72	3.0	14.044
SRM983	206/208	10	90.00	25	73.424
	206/204		-----[b]		2690

[a]Data not corrected for mass discrimination. Reported value is the average for the indicated number of injections.

[b]^{204}Pb not detected above background noise.

gives the isotope ratios measured for four different lead samples with flow injection of 1.0 mL samples of 500 ng L^{-1} solutions. The ratios were acquired by multiple ion monitoring of the four lead peaks for 16 seconds after the elution of lead reached a maximum, i.e., a total of four seconds on each isotope.

Spectral Interferences

Interferences due to background peaks in the ICP-MS spectrum have been well-characterized and pose some limitation in the analysis of a few elements, e.g., $^{40}Ca^{+}$ coincides with $^{40}Ar^{+}$ (20). In the case of overlap between analyte peaks, there is usually an isotope for most elements which will be free from overlap, or proper deconvolution techniques can be used to extract the needed analytical information. A more difficult interference to correct for is caused by the formation of MO^{+} and M^{2+} ions.

The MO^{+} signals are partly due to undissociated compounds in the plasma. Such elements as Ba, Sr, Ti, V, Y, the rare earths, Th and U, form strong M-O bonds with dissociation energies of 4 to 9 eV (21), and are believed to survive in the ICP to some extent (20). But the extent to which these ratios, MO^{+}/M^{+}, vary from instrument to instrument suggests that the MO^{+}/M^{+} ratio is also dependent on the ion sampling characteristics of the supersonic nozzle. It is desirable to maintain the residence time of extracted metal ions in the expansion stage to a minimum, thus decreasing the time in which recombination reactions can

occur. It is also desirable to maintain the local gas temperature around the skimmer high enough to minimize condensation and oxide formation but not so high that multiply charged ions are formed. Figures 7a and b show that the ThO^+/Th^+ ratio varies with plasma operating conditions, e.g., aerosol gas flow rate and forward power (without correction for mass discrimination). In the normal operating range of these parameters in our instrument, the ThO^+/Th^+ ratio remains $\lesssim$ 5%, and under conditions for maximum Th^+ signal, i.e., 0.4 L/min aerosol gas flow and 1.1 kW forward power, the ratio is $\lesssim$ 1%. The bond dissociation energy of ThO is 8.5 eV (21), and ThO^+ is the most stable of the metal oxide species we have observed so far. Therefore, our ion extraction device suppresses MO^+ ions efficiently (20). When the aerosol gas flow rate is increased, the molecule's residence time in the plasma is decreased and the gas temperature in the central channel probably also decreases. For these reasons, the detected ratio ThO^+/Th^+ should increase with aerosol gas flow rate. This behavior is observed in Figure 7a. As forward power increases, the plasma would be expected to become "hotter" and to dissociate metal oxide species more effectively as shown in Figure 7b.

Those elements with low second ionization energies ($\lesssim$ 12 eV) are also observed to form doubly charged species. The extent to which doubly charged metal ions are formed in the ICP is predicted by the Saha equation and depends upon second ionization energy, electron number density (n_e) and ionization temperature (T_{ion}) (22). The Th^{2+}/Th^+ ratio

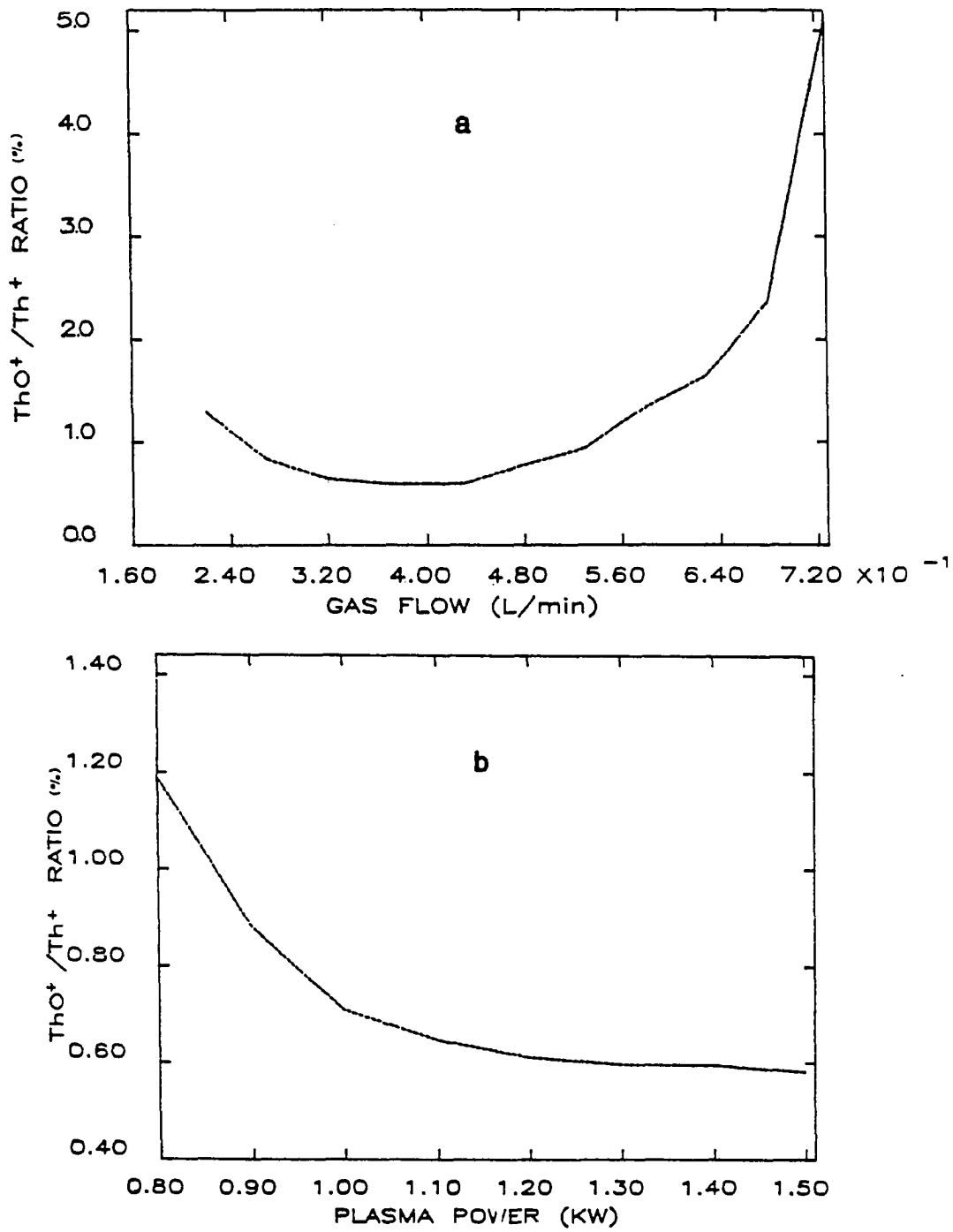

Figure 7. Dependence of ThO^+/Th^+ on: a) aerosol gas flow rate; b) plasma forward power

is predicted to be ~0.06 in the ICP at $n_e = 10^{15}$ cm^{-3} and $T_{ion} = 7500°K$ (7). Figures 8a and b show the dependence of Th^{2+}/Th^{+} on aerosol gas flow rate and plasma forward power (without correction for mass discrimination). Note that the behavior observed in these curves is opposite to the expected, i.e., with increase in aerosol gas flow rate n_e and T_{ion} in the central channel should decrease, along with analyte residence time. This should translate to lower efficiency for doubly charged ion formation. Also, with higher forward power n_e and T_{ion} should increase, and, therefore, doubly charged species should become more prominent. This contradiction in experimental versus expected behavior is believed to be a manifestation of a "pinch" discharge at the nozzle orifice, i.e., an electrical breakdown of the gas to the nozzle (1). This phenomenon is also believed to be the cause for the observed dependence of ion kinetic energies on ICP operating parameters (7). The extent to which this discharge occurs also depends on ion extraction characteristics, e.g., increasing the nozzle diameter decreases the effects due to the pinch (23).

Though empirical ways have been found to attenuate the pinch discharge (24), it is worthy to note that this phenomenon may also be attributed with maintaining the MO^{+}/M^{+} ratios low during the ion extraction process. Thus, total removal of the pinch may eliminate the formation of doubly charged species in the extraction but may also allow for higher oxide formation. It may be desirable to be able to control the

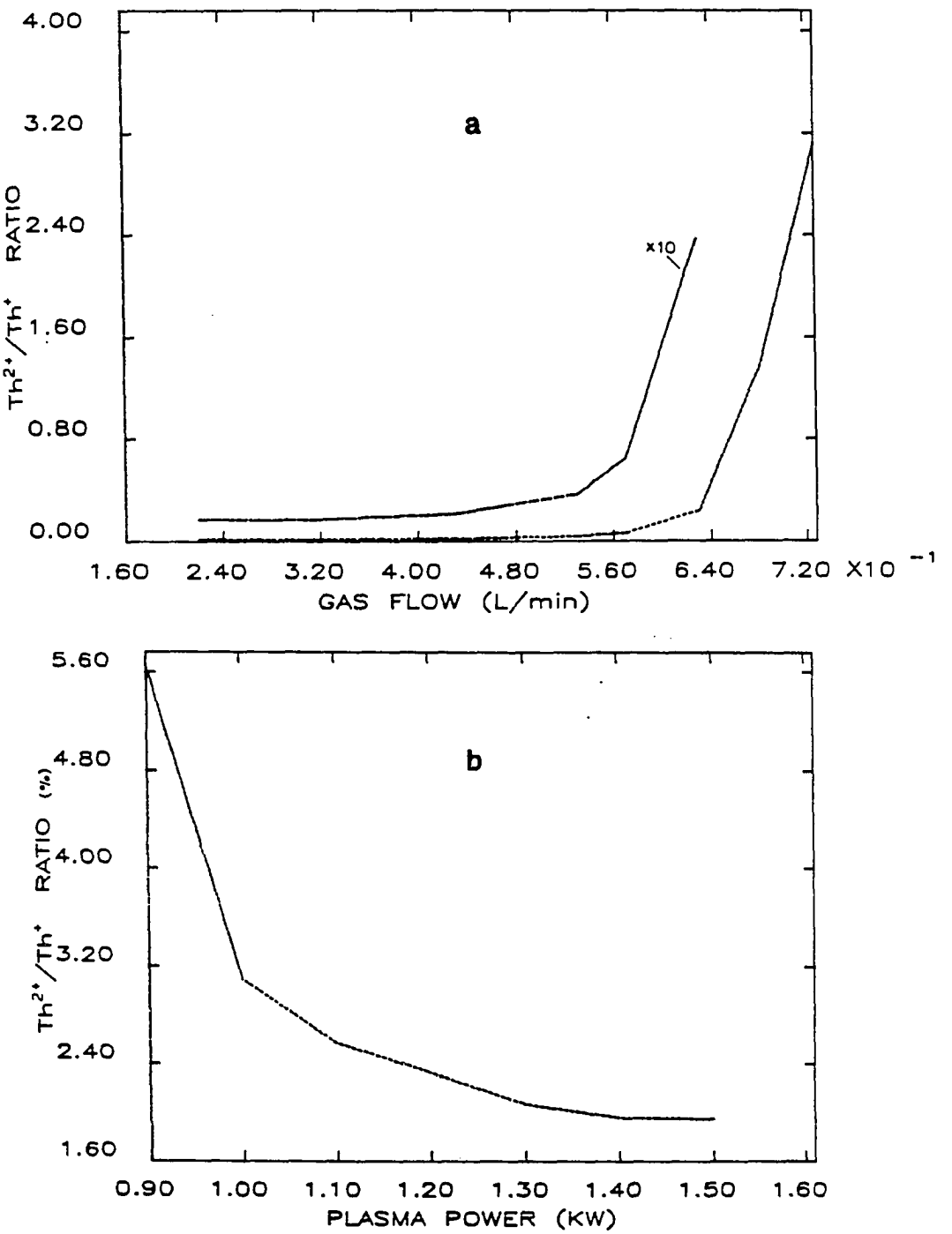

Figure 8. Dependence of Th^{2+}/Th^{+} on: a) aerosol gas flow rate; b) plasma forward power

amount of "pinch" for a particular analysis, therefore controlling the amount of allowed spectral interference from metal oxides and doubly charged ions.

CONCLUSION

The description of the ICP-mass spectrometer instrument presented above points out some of the problems found in the development of this analytical tool: a) sampling interface arrangements which will give an intense and "true" representative sample of the ion population in the plasma; b) proper ion focusing and detector arrangement in order to more efficiently detect the large ion currents existing in the ICP; and c) the possibility of controlling the extraction process to minimize spectral interferences and ultimately enhance the analytical signal. The present analytical capabilities of ICP-MS are but a manifest of the compromises made in the quest for efficient ion sampling, focusing and detection. Only continued research in the development of ICP-MS will show the ultimate limitations and capabilities of this technique for elemental analysis.

LITERATURE CITED

1. Houk, R. S.; Fassel, V. A.; Flesch, G. D.; Svec, H. J.; Gray, A. L.; Taylor, C. E. Anal. Chem., 1980, 52 2283.

2. Kantrowitz, A.; Grey, J. Rev. Sci. Instrum. 1951, 22, 328.

3. Gray, A. L.; Date, A. R. Analyst 1983, 108, 1033.

4. Douglas, D. J.; Quan, E. S. K.; Smith, R. G. Spectrochim. Acta, 1983, 38B, 39.

5. Allen, J. D. Jr.; Wolfe, J. P.; Schweitzer, G. K. Int. J. Mass Spectrom. Ion Phys. 1972, 8, 81.

6. Allen, J. D., Jr.; Durham, J. D.; Schweitzer, G. K.; Deeds, W. E. J. Electron Spectrosc. Relat. Phenom. 1976, 8, 395.

7. Olivares, J. A.; Houk, R. S. Appl. Spectrosc., submitted (1985).

8. McGilvery, D. C. Ph.D. Dissertation, LaTrobe University, 1968.

9. Delmore, J. E. Int. J. Mass Spectrom. Ion Proc. 1984, 56, 151.

10. Höglund, A.; Rosengren, L-G. Int. J. Mass Spectrom. Ion Proc. 1984, 60, 173.

11. Yoon, S.; Knuth, E. L. "Progress in Astronautics and Aeronautics"; S. S. Fisher (Ed.); American Institute of Aeronautics and Astronautics: New York, 1981; Part II, p. 867.

12. Campargue, R. "Rarefied Gas Dynamics, Proc. 4th Int. Symp. Rarefied Gas Dynamics"; J. H. de Leeuw (Ed.); Academic Press: New York, 1966; Vol. II, p. 279; French, J. B.; O'Keefe, D. R. "Rarefied Gas Dynamics, Proc. 4th Int. Symp. Rarefied Gas Dynamics";

J. H. de Leeuw (Ed.); Academic Press: New York, 1966; Vol. II, p. 299; Fenn, J. B.; Anderson, J. B. "Rarefied Gas Dynamics, Proc. 4th Int. Symp. Rarefied Gas Dynamics"; J. H. de Leeuw (Ed.); Academic Press: New York, 1966; Vol. II, p. 311.

13. Pertel, R. Int. J. Mass Spectrom. Ion Proc. 1975, 16, 39.

14. Ashkenas, H.; Sherman, F. S. "Rarefied Gas Dynamics, Proc. 4th Int. Symp. Rarefied Gas Dynamics"; J. H. de Leeuw (Ed.); Academic Press: New York, 1966; Vol. II, p. 84.

15. French, J. B. "Molecular Beams for Rarefied Gasdynamic Research", W. C. Nelson (Ed.); NATO-AGARD Fluid Dynamics Panel, 1966; AGARDograph 12.

16. Kalnicky, D. J.; Fassel, V. A.; Kniseley, R. N. Appl. Spectrosc. 1977, 31, 137.

17. Hayhurst, A. N.; Kittelson, D. B.; Telford, N. R. Combust. Flame 1977, 28, 123.

18. Darcie, T. E., Institute for Aerospace Studies, University of Toronto, UTIAS Report No. 269 1983.

19. Goodings, J. M.; Karellas, N. S. Int. J. Mass Spectrom. Ion Proc. 1984, 62, 199.

20. Douglas, D. J.; Houk, R. S. Prog. Anal. Atomic Spectrosc., in press 1985.

21. Gaydon, A. G. "Dissociation Energies and Spectra of Diatomic Molecules"; Chapman and Hall: London, 1968; Ch. 12.

22. Houk, R. S.; Svec, H. J.; Fassel, V. A. Appl. Spectrosc. 1981, 35, 380.

23. Gray, A. L. Department of Chemistry, University of Surrey, Guilford, England, private communication, 1985.

24. Douglas, D. J. SCIEX Inc., patent pending 1985.

SECTION II.

KINETIC ENERGY DISTRIBUTIONS OF POSITIVE IONS IN AN INDUCTIVELY COUPLED PLASMA MASS SPECTROMETER

INTRODUCTION

Despite the considerable recent interest in inductively coupled plasma-mass spectrometry (ICP-MS) as an analytical technique for elemental and isotopic analysis (1), as yet comprehensive measurements of kinetic energies for ions detected from the ICP have not appeared in the literature. The ion kinetic energy distribution is an important parameter to be characterized for any ion source in that it influences ion collection, focusing, and mass analysis. Such measurements may also yield interesting fundamental or diagnostic information about the ICP itself or any perturbation induced upon the plasma by the presence of the metal cone containing the sampling orifice. As an example of the latter, early attempts to employ continuum sampling for ICP-MS were plagued by formation of an electrical discharge (termed the pinch effect (2)) between the plasma and the sampling orifice. The deleterious effects of the pinch include orifice erosion, high background levels, multiply charged ion formation, detection of ions from the sampling cone, and poor peak shapes characteristic of energetic ions. Although empirical ways have been found to attenuate these effects (3,4) at least with our apparatus some residual pinch persists. Characterization of the ion kinetic energy distribution and its dependence on various plasma operating parameters could yield some information about the causes of this phenomenon.

Traditionally, the kinetic energy distributions of ions in plasmas and flames have been studied by extracting ions into a vacuum system containing a retarding grid upstream from a quadrupole mass analyzer (5-7). Such methods require extensive error treatment in order to correct for concentration effects due to mass discrimination caused by the mean velocity of the jet expansion into the vacuum chamber and potential effects which perturb the ion kinetic energy distributions (7). These error treatments are particularly useful when extracting data from experiments which are subsequently used for the quantitation of concentration and temperature profiles in the plasma or flame.

Recently Darcie (8) has employed the retarding grid method for the characterization of the source emittance of an atmospheric pressure corona discharge ion source. He describes a theoretical treatment (9) based on the Boltzmann equation which is in good agreement with the experimentally determined axial and radial ion velocity distributions from such a source. In order to separate the axial and radial velocity components from the measured kinetic energy of an ion, it is necessary to determine the angle at which the ion is moving with respect to the z-axis of the jet expansion. This means that the plane retarding grid must have a small point of entry and be able to move about the x or y axis. The detector must also be able to follow this movement. Such an apparatus can give much useful information about the coupling of a quadrupole mass analyzer to a jet expansion source, but the equipment is complicated in design and may have little if any other use.

For qualitative information on the effect of different plasma parameters on ion energy distributions, it may be sufficient to apply a retarding potential to the ion path using the dc quadrupole rod bias. This approach was used by Gray and Date (3), who determined the energy spread of cobalt ions to be 7.5 eV in their ICP-mass spectrometer using a continuum flow sampler under a particular set of ICP conditions. As these authors point out the measured energy spread is not sufficient to require energy analysis before mass analysis, though this value is greater by over a factor of three than the ion energy spread from boundary layer samplers (2). Gray and Date, though, did not point out that the energy distributions of ions from an ICP are affected by plasma operating parameters when using a continuum flow sampler. Experiments with continuum flow ion extraction for our ICP-mass spectrometer indicate that the ion energy distributions detected are dependent on the various gas flow rates, forward power, and sampling position. These effects on the ion energy distributions also influence the sampled ion signal. Generally, when the ion energy increases the signal decreases and the peak shapes deteriorate. In this work, we present the results of the energy analysis of positive ions in an ICP, and the effects that different plasma operating parameters have on the kinetic energy distributions.

APPARATUS AND PROCEDURES

Instrumentation

The ICP-mass spectrometer and techniques used in this study are shown in Figure 1. Solutions are nebulized with an ultrasonic nebulizer (G) (10), desolvated (H), and introduced into the ICP via the aerosol gas flow (E). A fraction of the ions formed in the plasma are extracted through a continuum flow sampling interface similar to that described by Gray and Date (3) and Douglas and French (11). The plasma flows around the tip of a Ni sampling cone (I) with a 0.53 mm diameter circular orifice drilled in its tip. This orifice is large enough to draw gas directly from the plasma by puncturing the boundary layer formed between the plasma and the sampling cone (2,3). The majority of the sampled gas flowing into the first stage of a 3-stage differentially pumped vacuum chamber is pumped away by a 10 L/s mechanical pump (T). The pressure measured at this stage by a Convectron gauge (Granville Phillips, Boulder, Colorado) is ~1.5 torr. This first chamber includes a viewing port to permit visual observation of the luminous expanding jet formed in the extraction process. The central core of the free jet expansion is passed into the second vacuum stage through a 1.40 mm diameter hole in a sharply tipped stainless steel skimmer (J). Both the sampler and the skimmer are electrically grounded along with the rest of the vacuum chamber. The separation between the sampler and skimmer tip is approximately 9 mm. The design of the sampler and skimmer follow the details pointed out by Pertel (12). The second stage is pumped by a 1600 L/s

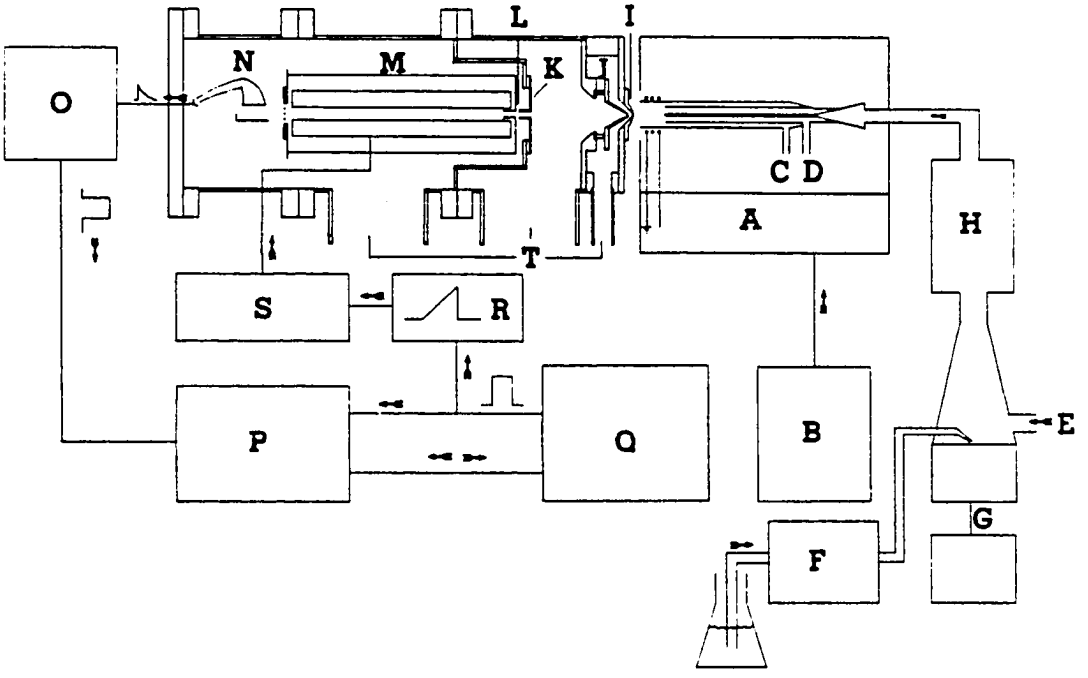

Figure 1. Experimental apparatus: (A) ICP, torch and impedance matching network; (B) 27.12 MHz RF generator; (C) inlet for the argon outer gas; (D) inlet for the argon auxiliary gas; (E) inlet for the argon aerosol gas; (F) peristaltic pump for solution uptake; (G) ultrasonic nebulizer and power supply; (H) desolvation apparatus; (I) nickel sampling cone; (J) stainless steel skimmer; (K) differential pumping plate; (L) ELFS lens; (M) quadrupole mass analyzer; (N) Channeltron electron multiplier; (O) current to frequency converter; (P) signal averager; (Q) microcomputer; (R) 0-50 V dc ramp generator; (S) quadrupole control electronics

oil diffusion pump (T). The pressure measured in this stage by a cold cathode gauge is 3×10^{-4} torr under normal operating conditions. An ion lens normally resides in this stage but has been removed for these experiments to minimize disturbance of the jet expansion. The differential pumping plate (K) separating the second stage from the third contains a 6.4 mm diameter by 12.8 mm long tube and is on axis with the orifice (I), skimmer (K), and quadrupole mass analyzer (M) which resides in the third stage. The differential pumping plate is about 10 cm from the tip of the skimmer. The gas jet is, therefore, allowed to expand through this distance. The differential pumping plate is isolated from ground and biased at -220 V dc; thus, it serves as an ion lens. Ions sampled from the plasma and passing through the skimmer are accelerated towards this plate. In the initial stages of the jet expansion the local pressure is still rather high, the mean free path is small, and frequent collisions occur. As the pressure in the jet drops axially, the ions experience fewer collisions and their velocity increases due to the electrostatic acceleration towards the plate (9).

The ions are focused by the differential pumping plate into the third stage. They then traverse a second ion lens (L) (called the "ELFS" lens, a registered trademark of Extranuclear Laboratories, Pittsburgh, PA) kept at -20 V dc which is the entrance into the Extranuclear quadrupole mass spectrometer (M). Ions of a selected mass pass through the mass spectrometer and are detected by a Galileo 4870 Channeltron electron multiplier (N) (Galileo Electro-Optics Co., Sturbridge,

MA) operated in the analog mode and set at a bias voltage of either -2500 V dc (for H_2O^+ and Co^+) or -2200 V dc (for Ar^+). The third stage is pumped by a 1600 L/s oil diffusion pump with a liquid N_2 trap (T). The pressure in this stage is measured by an ionization gauge and is 1.5 x 10^{-5} torr.

A stopping potential is applied to the paths of the ions entering the quadrupole by setting the rod bias at a positive dc potential. The rod bias potential is provided by a sawtooth 0-50 V dc ramp (R) from an oscilloscope which is synchronized to a signal averager (P) (Model 1170 Nicolet Instrument Co., Madison, WI) under computer control. Both instruments are triggered under program control from a PDP-11/03 microcomputer (Q) (Digital Equipment Co., Merrimack, NH). The analog output of the electron multiplier is passed through a current to frequency converter (Analog Technology Corporation, Pasadena, California) (O). The pulses from the converter are counted and stored by the signal averager in a 4096 channel memory. Each sweep lasts approximately 20 seconds and two to four sweeps are averaged. The averaged energy spectrum is stored by the computer for later analysis. No attempt was made to calibrate the energy scale, therefore the data shown can only be trusted as qualitative measurements of the ion energy trends with changes in plasma parameters.

Radial and axial profiles of ion signal and kinetic energy were recorded by translating the plasma in the x and z directions respectively relative to the stationary sampling orifice (I).

Data Analysis

The collected energy spectra represent ion intensity as a function of rod bias voltage. These plots resemble S-shaped curves such as that shown in Figure 2. In principle, the first derivative of this curve yields the ion energy distribution. The average ion kinetic energy ($\overline{KE}$) is characterized by the voltage at which the maximum of the first derivative occurs (the center of the curve). The kinetic energy spread (ΔKE) is the width of the first derivative at half height, which comprises approximately 75% of the area of the derivative curve. Such an analysis is difficult with real data because the noise is amplified by a first derivative calculation by differences. The data normally require a great deal of smoothing before the first derivative can be calculated (13). The presence of an occasional spurious spike in the data (such as that shown in Figure 2) can unduly bias the first derivative calculation.

In order to overcome this problem, a simple algorithm was used which provided both a measure of the kinetic energy distribution of the ions and fast determination with some operator control over the fit. A computer program was written with interactive graphics which allows the operator to select areas of interest in the real data plot (i.e., the S-curve) by marking the areas with hairline cursors (see Figure 2). The operator selects the top of the S-curve and the computer draws a straight line through the mean of the points selected. This is called the "100%" line. The bottom of the S-curve is selected and the computer

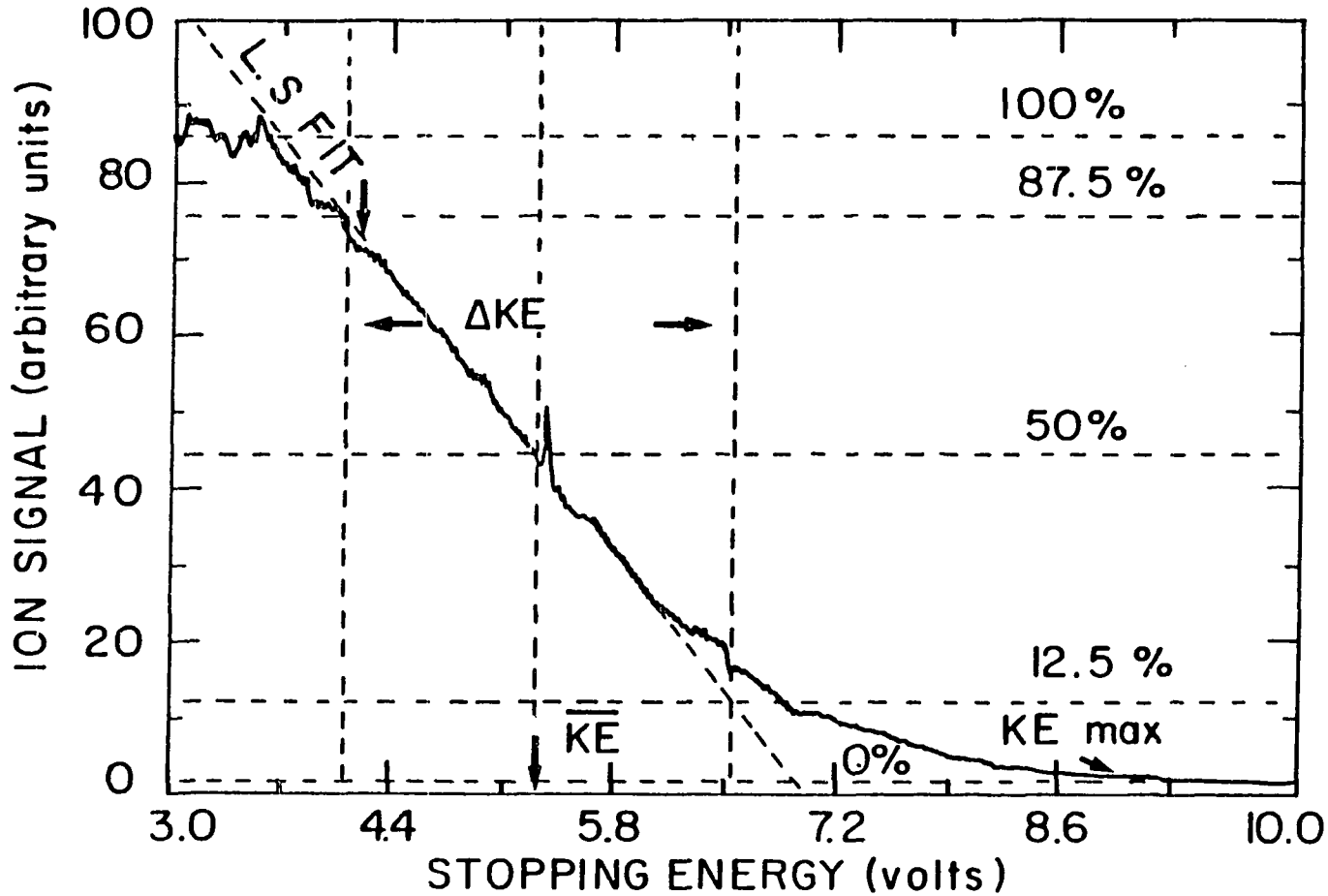

Figure 2. Dependence of Ar^+ signal on bias voltage applied to the quadrupole rods bias. The lines used in the algorithm to determine the ion kinetic energy distributions are shown (see text)

again draws a straight line through the mean; this is called the "0%" line. Then, the steepest portion of the curve is selected and the computer performs a least squares (LS) fit to a line through these points; this is the "LS fit" line. The program then draws horizontal and vertical lines through the points intersecting the "LS fit" line at 12.5%, 50.0%, and 87.5% of the range marked by the "100%" and "0%" lines. The voltage at which the "50.0%" line intersects the "LS fit" line is taken to be the center of the normal distribution curve, $\overline{KE}$. The difference between the voltages marked by the 87.5% and the 12.5% lines is ΔKE. The area marked by these points is approximately equal to 68% of the normal distribution curve or one standard deviation from the mean. The operator also selects the applied voltage at which the ion signal is fully suppressed, i.e., the foot of the S-curve, which is denoted the "maximum ion kinetic energy", KE_{max}. These results are stored, for each parameter change, for later interpretation and plotting. The results from this simple algorithm yield kinetic energy values that are essentially equivalent (within experimental error) to those calculated from the more rigorous first derivative method.

The "100%" and "0%" lines determined in the above procedure also give information about the ion signal and background for each variation of the parameter under study; therefore, ion signal distribution curves are included. The background signal from the plasma was substantial in these experiments ($\sim 5 \times 10^5$ counts s^{-1}) because the optical baffle normally placed in the ion lens was removed allowing much of the light from

the ICP to reach the multiplier. Therefore, the background ("0%" line) at the mass of interest was subtracted from the signal ("100%" line).

Table I lists the normal settings for each parameter studied in these experiments when that parameter was not the variable.

Table I. Experimental Parameters

Plasma outer argon gas flow rate	17 l/min
Auxiliary argon gas flow rate	0.5 l/min
Aerosol argon gas flow rate	0.43 l/min
Plasma forward power	1.1 kW
Solution uptake to nebulizer	1.8 ml/min
Sampling position	7 mm above load coil Sampler centered on axial channel

RESULTS AND DISCUSSION

Data were collected for three ions, namely, Ar^+ and H_2O^+ from the background and Co^+ from a 10 mg L^{-1} solution. The average kinetic energy distributions measured for these three ions were quite similar for a particular set of plasma parameters, as shown in Figure 3. Therefore, the data shown below are for Ar^+ ions, and unless otherwise stated, the behavior of H_2O^+ and Co^+ was similar to that for Ar^+. Some experiments were done without nebulization or aerosol gas flow. Naturally, the H_2O^+ signal was weak and not measured and Co^+ was absent in these cases. In general, a change in some plasma parameter that caused the $\overline{KE}$ to increase also displaced the entire energy distribution to higher energies so that both the ΔKE and KE_{max} tended to increase as well. For simplicity we therefore show only the measured $\overline{KE}$, unless otherwise indicated.

It is instructive to note the effects of the simple two element ion lens on the detected ion energies. Figure 4a indicates that voltages in the range -250 to 0 V dc applied to the first lens, (K, Figure 1), i.e., the differential pumping plate, have no observable effect on the measured kinetic energy. When the potential on this first lens is made positive the signal for Ar^+ is large and the energy distribution increases linearly with applied voltage. A positive potential on this lens would normally be expected to simply stop ions and prevent their transmission to the mass analyzer. Apparently, with positive voltages on the differential pumping plate the ions are being slowed down in a

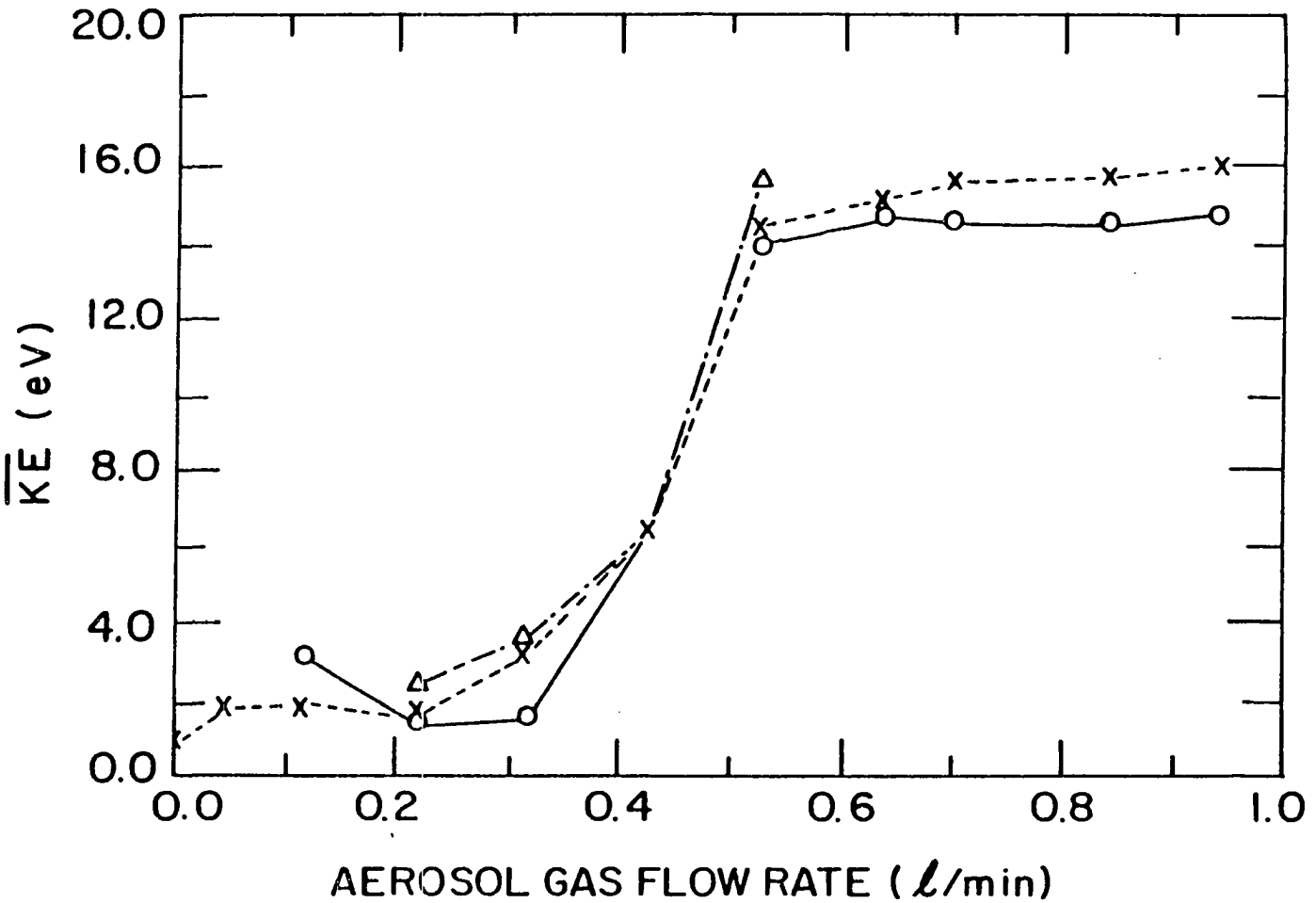

Figure 3. Change in ion average kinetic energy with aerosol gas flow rate for a) (o) Ar^+; b) (x) H_2O^+; c) (Δ) Co^+

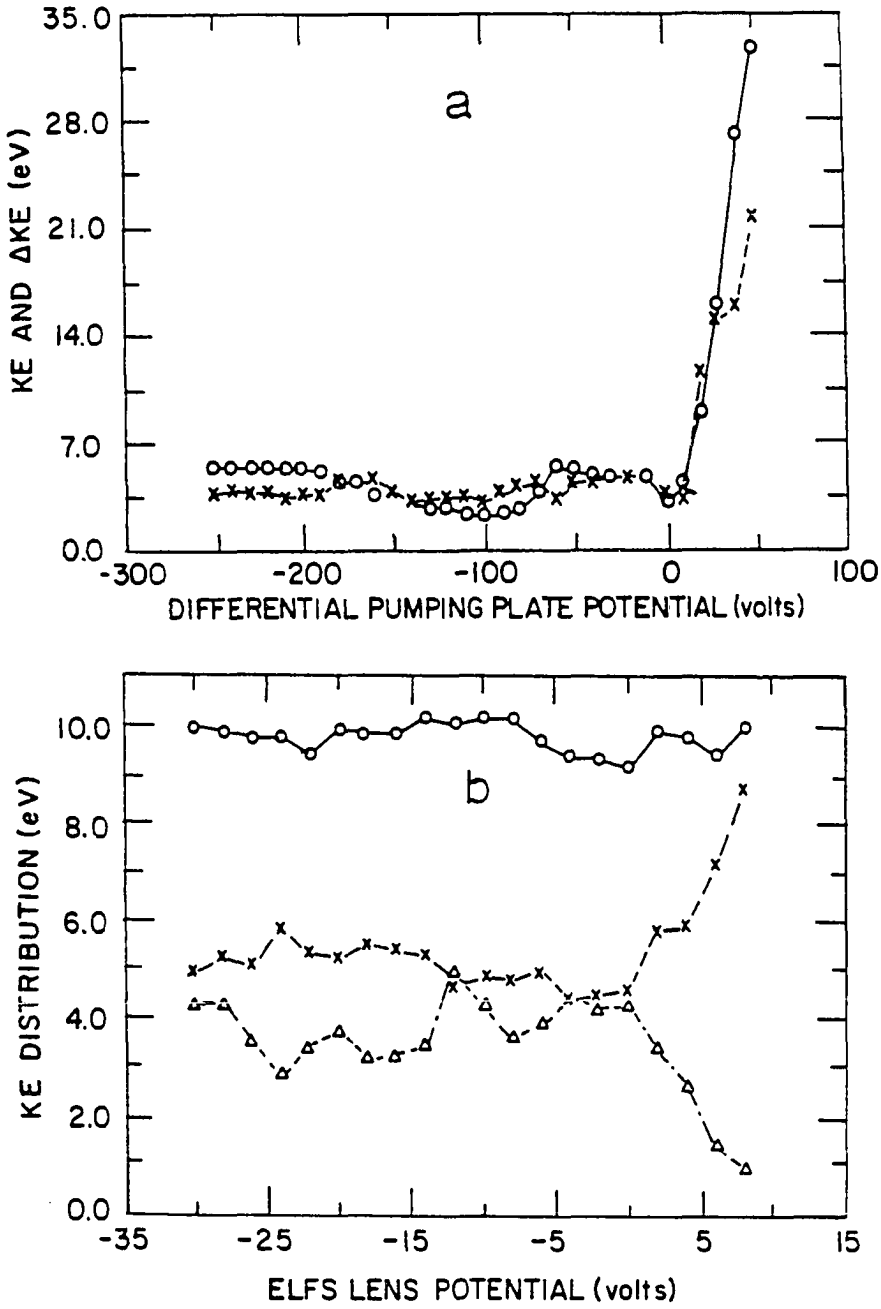

Figure 4. Change in Ar^+ kinetic energy distribution with applied potential on: a) differential pumping plate, (o) $\overline{KE}$, (x) ΔKE; b) ELFS lens: (o) KE_{max}, $\overline{(x)}$ KE, (Δ) ΔKE

region where collisions still occur. The neutral gas from the jet expansion collides with and transfers momentum to the retarded ions, forcing them to penetrate into areas of high positive potential. The momentum gained by the ions that undergo forward collisions results in a measurable gain in kinetic energy to values equal to the retarding potential, thus the ions penetrate the retarding barrier and continue to the mass spectrometer. The entrance to the quadrupole rods, the ELFS lens (L, Figure 1), resides in the third vacuum stage where the pressure is much lower and gas collisions are no longer significant. As the voltage applied to the quadrupole entrance aperture varies between -30 to 0 V dc the detected ion energy remains constant (Figure 4b). When this voltage becomes positive KE_{max} remains constant, $\overline{KE}$ increases towards the maximum, ΔKE decreases towards zero, and the signal also decreases. Thus, the quadrupole entrance aperture behaves like a "normal" collision-free ion lens in that lower energy ions are cut off by a positive applied potential. The data described below were obtained with negative voltages on both lens elements so that these effects do not contribute to the determined ion energies.

Effects of Plasma Parameters on Ion Energy

As shown in Figure 3, ion energies tend to increase with aerosol gas flow rate. This increase is steepest between 0.4 and 0.5 L min^{-1}, which causes an increase of nearly 12 eV in average energy. Ion ener-

gies determined with electrical power to the ultrasonic nebulizer (i.e., with nebulized H_2O) are quite similar to those obtained with the nebulizer off (i.e., in the absence of nebulized H_2O), not shown. Thus, the presence or absence of aqueous aerosol has little effect on the kinetic energy of extracted ions. Furthermore, as aerosol gas flow rate increases the Co^+ ion signal peaks at about 0.43 L min^{-1}, while the background decreases asymptotically (Figure 5).

In contrast to the aerosol gas flow, the auxiliary gas flow rate has relatively little effect on ion kinetic energy. When this latter flow was changed from 0 to 1.2 L min^{-1}, the $\overline{KE}$ increased by only 3 eV. The same behavior was observed with or without nebulized H_2O.

The average ion kinetic energy decreased asymptotically to 6 eV as outer gas flow rate increased (Figure 6a). Again, similar behavior was observed in either the presence or absence of nebulized H_2O in the aerosol gas flow (Figure 6a,b). The dependence of ion energy on outer gas flow rate was also determined for an ICP without an axial channel, i.e., no aerosol gas. In this case, the ion energy distribution remained independent of outer gas flow rate with $\overline{KE}$ of 2 eV, ΔKE of 2.5 eV, and KE_{max} of 5 eV (Figure 6c). These latter values are considerably less than those obtained if the axial channel was present. Curiously, the Ar^+ ion signal and background increased with outer gas flow rate if the axial channel was present (Figures 7a and 7b). This trend was also observed for H_2O^+; the Co^+ signal remained relatively constant. Conversely, the Ar^+ ion signal decreased and the background remained con-

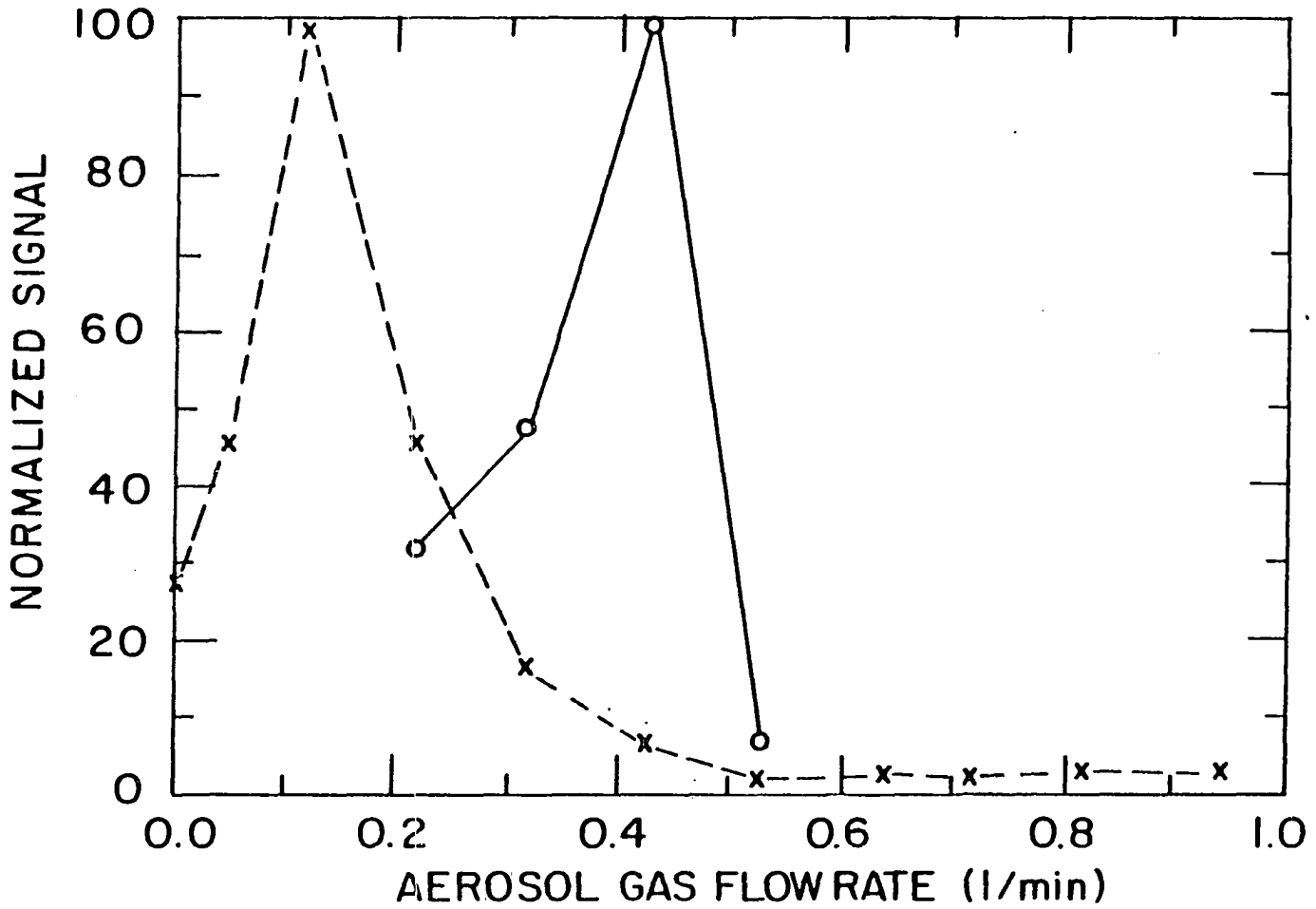

Figure 5. Change in (o) Co^{+} ion signal, and (x) background with aerosol gas flow rates

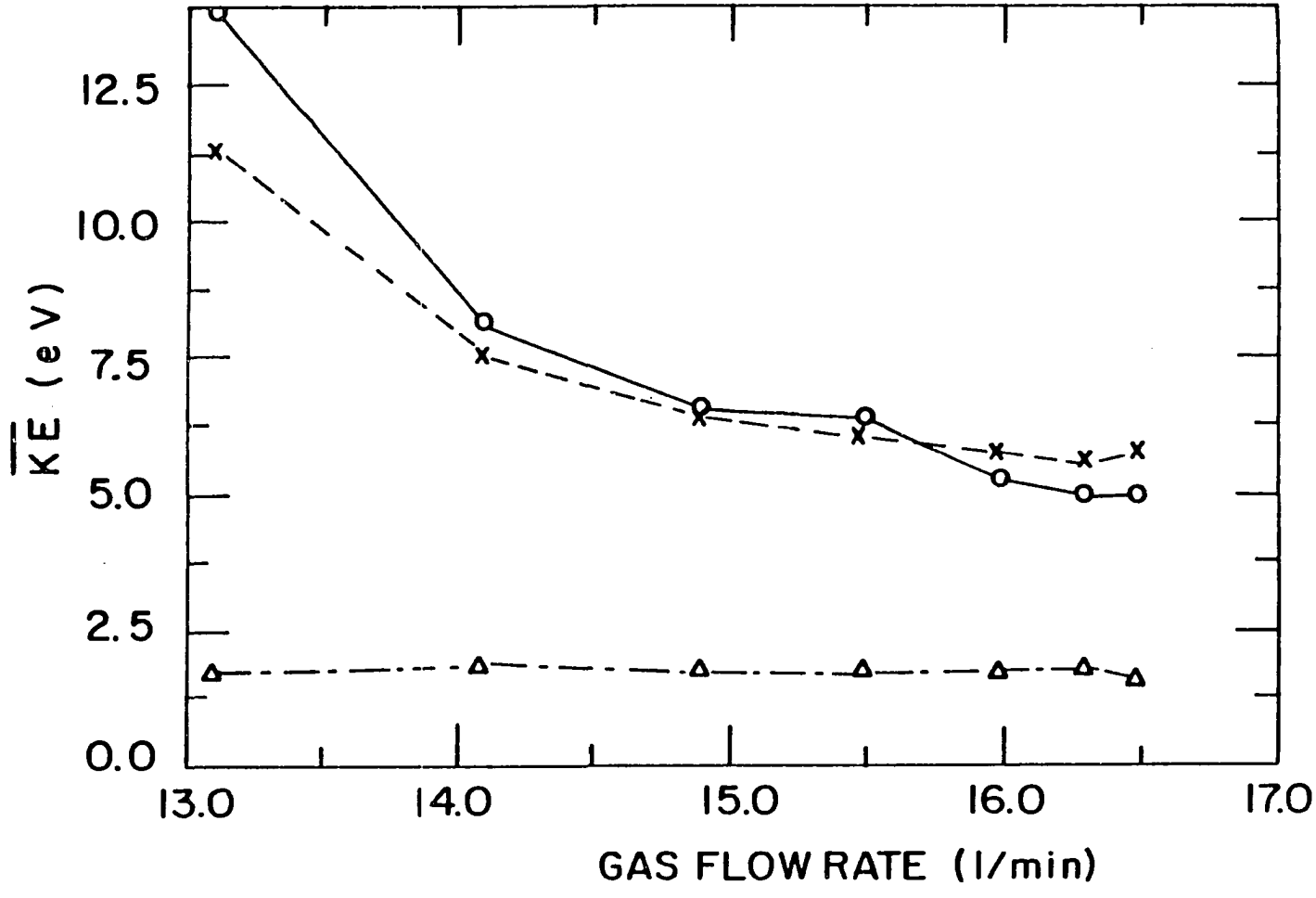

Figure 6. Change in Ar^{+} $\overline{KE}$ with outer gas flow rate: a) (o) with nebulization; b) (x) without nebulization; c) (Δ) without aerosol gas

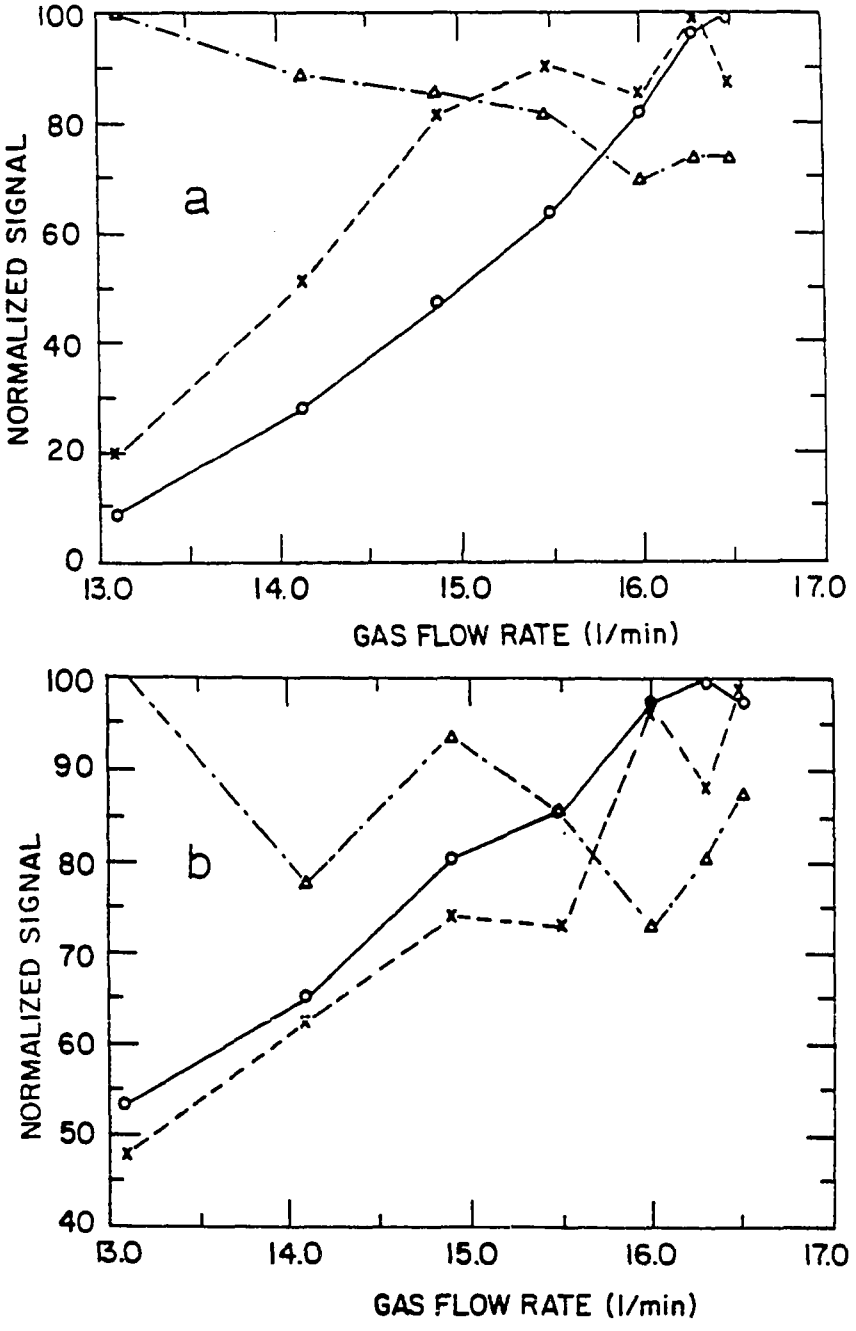

Figure 7 Change in signal with outer gas flow rate for: a) Ar^+; b) background: (o) with nebulization, (x) without nebulization, and (Δ) without aerosol gas

stant as outer gas flow increased if the axial channel was not present.

Increasing forward power supplied to the load coil caused the ion energy to decrease (Figure 8) in a similar fashion to that observed for the outer gas. As before, the presence or absence of nebulized H_2O had little effect on ion energy, while the ion energies observed with the axial channel present were several volts higher than without aerosol gas through the center of the plasma.

The kinetic energy of Ar^+ and Co^+ was determined with the sampling orifice positioned at various radial displacements relative to the plasma. The energy of Ar^+ remains essentially constant at radial positions between -4 and +4 mm (Figure 9). Within this range, the energy of Co^+ is similar to that shown for Ar^+ in Figure 9; furthermore, the intensity profile for Co^+ is bell-shaped and is much like that reported for In^+ by Gray and Date (3). It is interesting that ion energies are highest near the outer boundary of the ICP, i.e., at radii of 7-8 mm. This position is directly upstream from the plasma's induction region and corresponds approximately to one "skin depth" from the outer edge of the plasma (14).

Figure 10a illustrates that the energy of Ar^+ increases as the axial distance between the load coil and sampling orifice is increased. The rate of increase in ion energy is greatest from 22 to 26 mm from the load coil. This observation may be related to the audible and visible arc that occurs to any metal plate that is in front of the plasma and closer than 40 mm from the load coil. This discharge becomes less

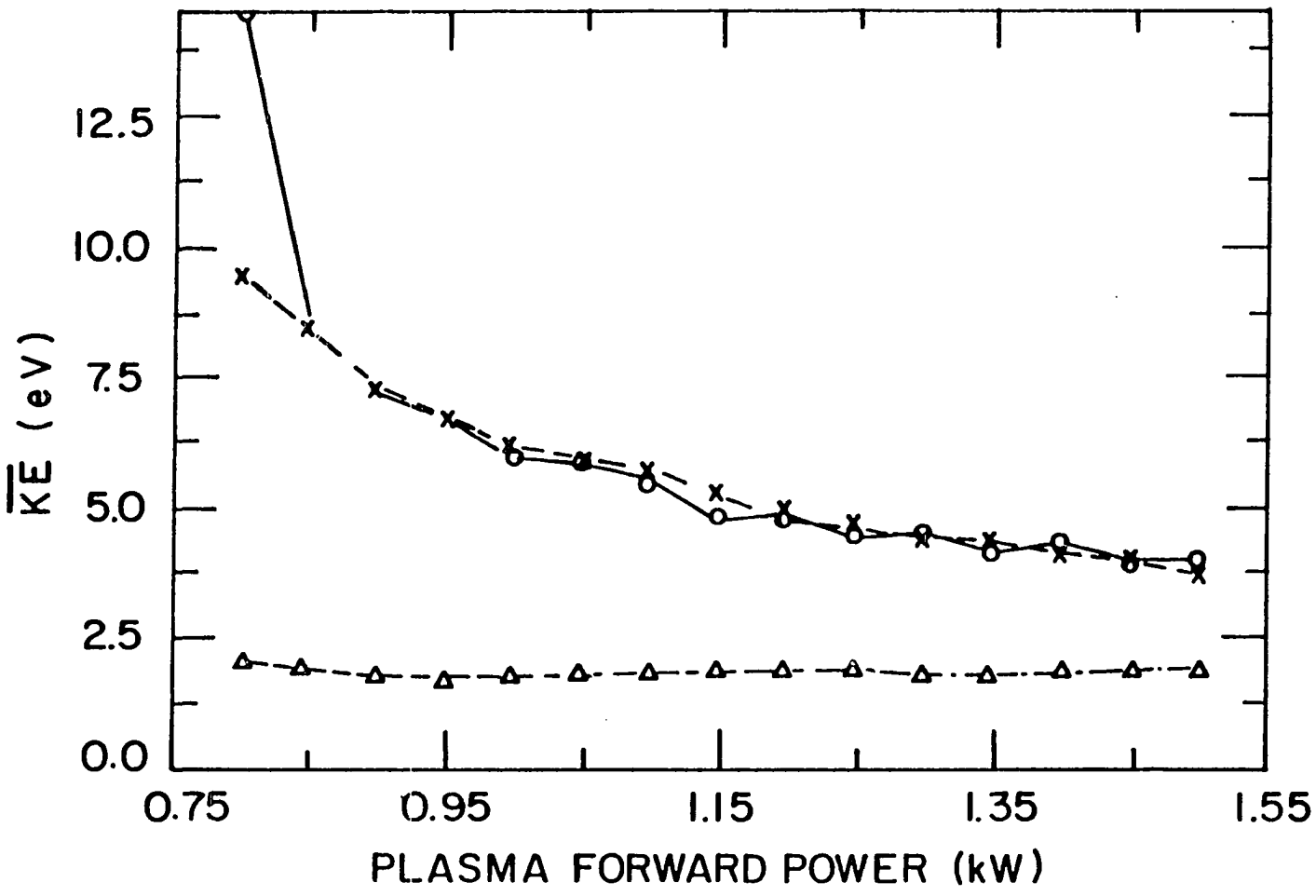

Figure 8. Change in Ar^+ $\overline{KE}$ with plasma forward power: (o) with nebulization, (x) without nebulization, and (Δ) without aerosol gas

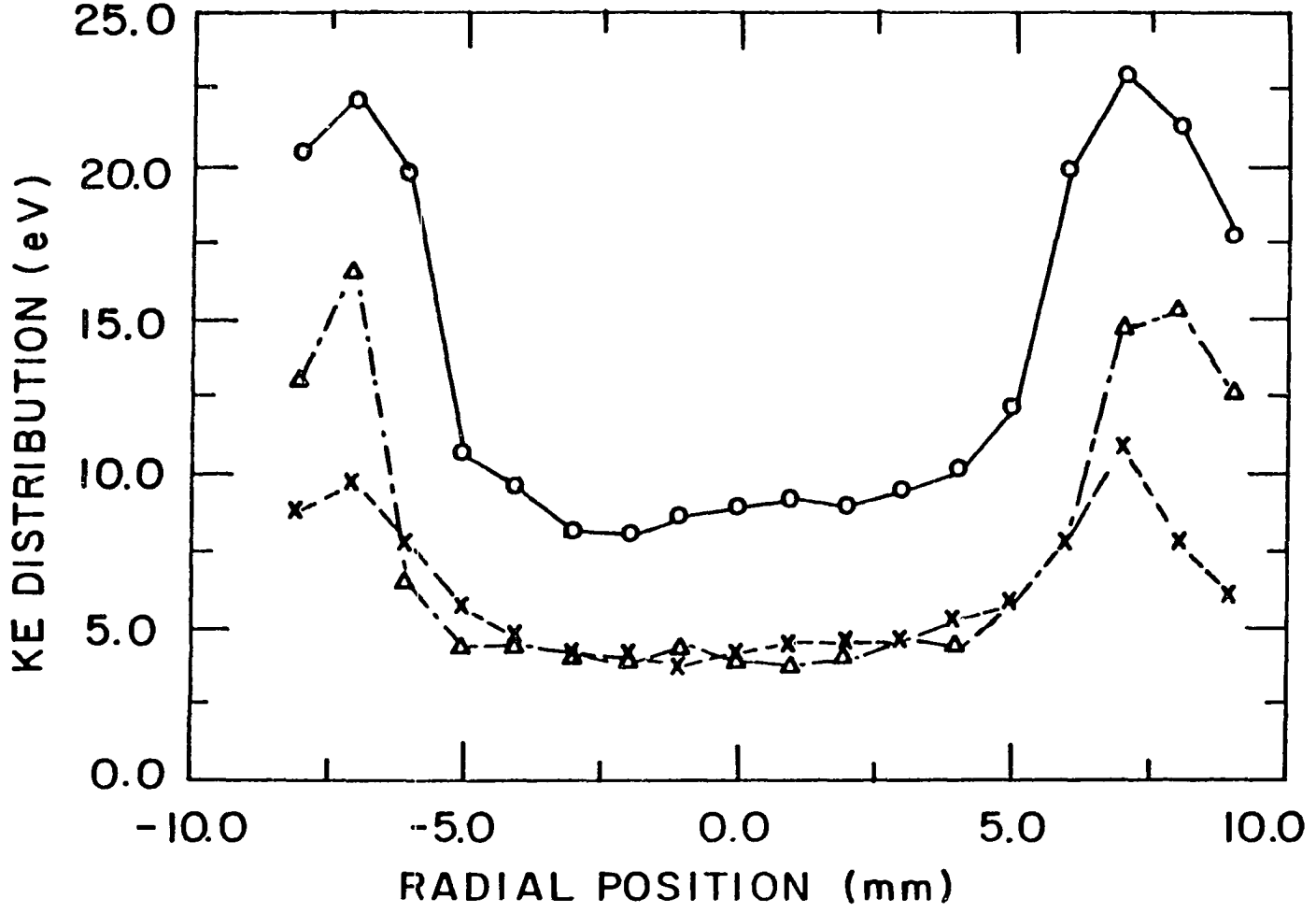

Figure 9. Kinetic energy distribution of Ar^+ with plasma radial position relative to the sampling orifice: (o) KE_{max}, (x) $\overline{KE}$, and (Δ) ΔKE

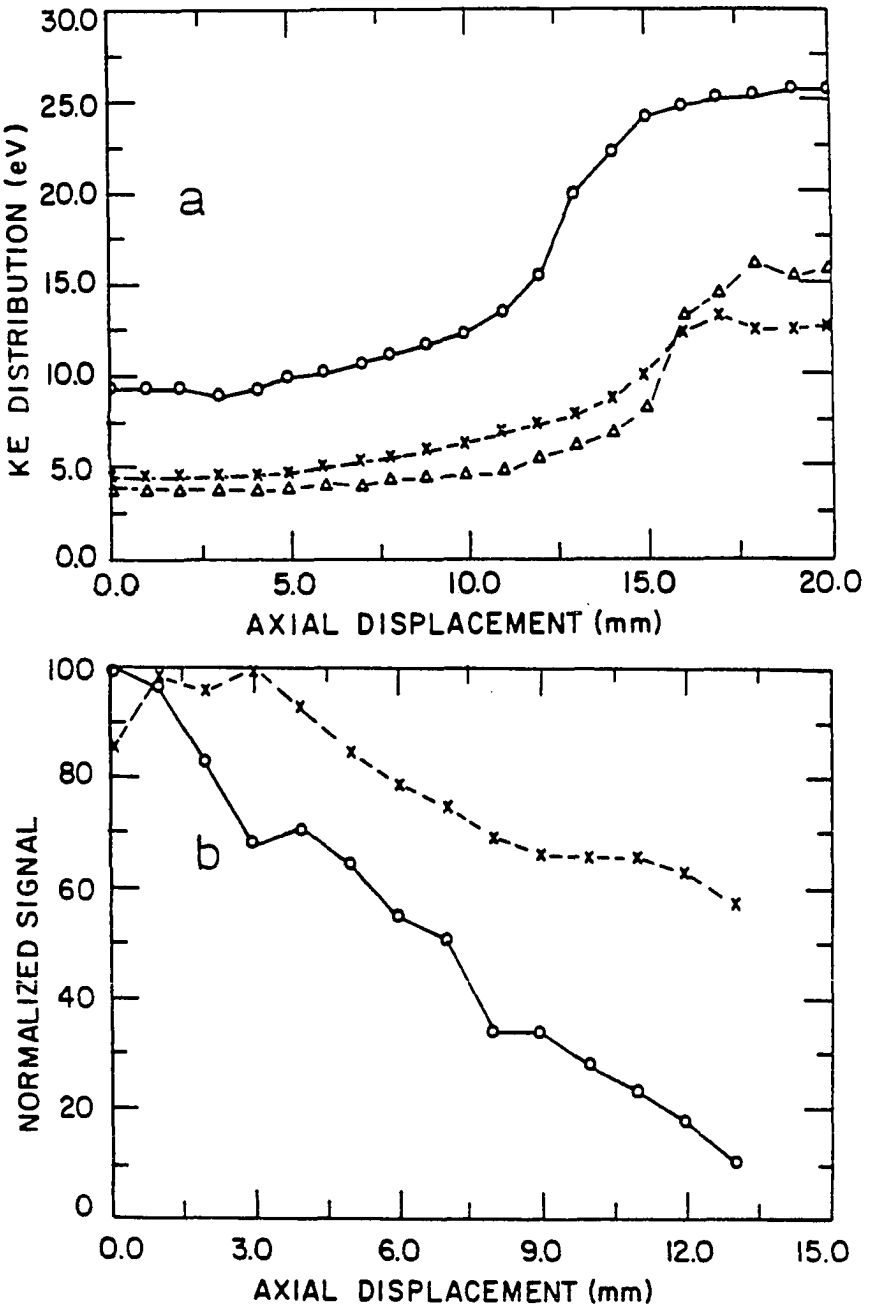

Figure 10. Effect of plasma axial displacement relative to the normal observation height (7 mm above the load coil) on: a) kinetic energy distribution of Ar^+, (o) KE_{max}, (x) $\overline{KE}$, and (Δ) ΔKE; b) (o) Co^+, and (x) background signal

noticeable as the metal object is moved closer and becomes immersed in the luminous white tip of the plasma. The energy of Co^+ depends on observation height in a similar fashion as Ar^+. However, the Co^+ signal decreases linearly as sampling height increases and cannot be discerned from background at heights beyond 19 mm above the load coil (Figure 10b).

Relation to Ion Extraction and Pinch Discharge

At this point, it is appropriate to compare the numerical values of ion kinetic energy described above with those expected from the simple thermal motion of atoms in the ICP. Under these conditions, the average kinetic energy of a particle would be expected to be approximately 3/2 kT_{gas}, which corresponds to 0.7 eV at 5000 K. The general magnitude of the ion energies observed here is considerably above this value. For example, under conditions we normally choose for analytical purposes ions can be readily transmitted through the rods if the latter are biased at +10 V. In fact, with our continuum sampling interface a positive rod bias is even beneficial in that cleaner, more symmetrical signal peaks with less splitting are observed than if the rods are biased negatively as would normally be done with a grounded source. Although during extraction the ions may be accelerated to supersonic velocities by collisions in the expanding jet, this process should not contribute more than 2 eV to the ion energy (15). Also, the observed ion energies should not vary much with plasma parameters if they were determined

primarily by the gas dynamic characteristics of the jet expansion. Clearly some other phenomenon is in effect that induces the 10 eV or so energies observed.

In this respect, an interesting aspect of these data is the tendency for ion energies to increase with aerosol gas flow rate (Figure 3). From simple thermal considerations the opposite behavior would be expected, i.e., increasing the aerosol gas flow rate should progressively "cool" the axial channel, thereby reducing temperature and electron density. Also, ion energy tends to decrease as forward power increases (Figure 8), which would otherwise be expected to induce a temperature increase in the ICP. We consider it likely that the positive ion energies observed are induced by a residual pinch discharge between the plasma and sampling orifice (1-3). If so, then it would appear that the intensity of the pinch increases with aerosol gas flow rate and decreases with forward power. Visual observation of the pink glow induced in the first vacuum stage by the pinch also corroborates this statement. The pink glow is not seen if there is no hole through the center of the plasma, which is consistent with the above concept that the pinch is associated with the presence of the axial channel. The physical basis for the pinch discharge being related to the hole through the center of the plasma is not clear at this time. However, it is interesting to note that other workers have also attributed the excitation and ionization properties of the ICP to its unique spatial structure, i.e., a "cool" axial channel surrounded and heated by a "hot" induction region.

Furthermore, species transport from the induction region to the axial channel is a crucial aspect of many of the models proposed for energy transfer in the ICP (16-22). One reason the ICP is remarkably free from interelement effects is that the electrical energy is added primarily to the induction region, the composition of which is not affected by changes in composition of the injected solution (23-26). ICP-MS with a continuum flow sampler should provide interesting diagnostic information about the ICP provided the pinch discharge is either absent or its effects on the observed spectra can be corrected for.

Finally, we attempted to determine whether the ion energies observed were correlated with the presence or absence of doubly charged ions in the mass spectra. Neither Ba^{+2} nor Ar^{+2} could be detected in sufficient quantity for further study under any of the plasma parameters used above. This is probably due to the low sensitivity of the instrument used for these experiments. Without an elaborate ion focusing lens and using dc detection our signal to noise ratio is ~100 for 10 mg L^{-1} Co under the operating conditions described in Table I. Separate studies (27) under similar operating conditions but with an ion focusing lens show that under normal operating conditions Th^{2+}/Th^{+} is 0.05; this ratio increases with aerosol gas flow rate. Similar trends are observed for other elements with low second ionization energies. With a "typical" ICP ionization temperature of 7500 K and electron density of 1×10^{15} cm^{-3} the Saha equation predicts Th^{2+}/Th^{+} to be ~0.06 if the partition functions of Th^{+2} and Th^{+} are assumed to be approximately

equal. Thus with our present instrument configuration and under the appropriate operating conditions the "pinch" can be minimized to give expected levels of doubly charged ions. Yet, as mentioned above at high aerosol gas flow rates the ionization temperature of the plasma and electron number density should decrease, and we observe (27) higher Th^{2+}/Th^{+} ratios under such conditions. The observed dependence of M^{+2}/M^{+} and ion kinetic energies on the aerosol gas flow rate are apparently manifestations of the residual "pinch" discharge present in our instrument.

On the other hand our present apparatus (27) yields rather low levels of MO^{+} ions from refractory metal oxides. For example, the observed ratio ThO^{+}/Th^{+} is $\lesssim 1\%$ for the operating conditions in Table I. Apparently, the residual pinch discharge present in our device is sufficiently intense to keep the sampled gas "hot" as it flows through the orifice, thus suppressing formation of MO^{+} during the extraction process. However, our residual pinch is not intense enough to yield any Ni^{+} from the sampling cone or excessive levels of doubly charged ions. Experimental techniques have recently been described for suppressing the pinch almost totally (4). In future ICP-mass spectrometers it may prove beneficial to be able to control and vary the intensity of the pinch. For example, it might be desirable to be able to induce a weak pinch to break up MO^{+} from rare earth elements or Ti, whereas other samples containing less refractory elements may not require special measures to dissociate oxide ions. Furthermore, the presence of a weak pinch may

facilitate finding a single set of operating parameters (sampling position, forward power, gas flow rates, etc.) that are appropriate for determination of a large number of elements in various sample matrices. While MO^+ formation and identification of "compromise" conditions for multielement analysis are not severe problems in current ICP-MS instruments there remains some room for improvement in these areas. Continued studies of the pinch phenomenon and the ion extraction process may thus lead to further improvements in the analytical figures of merit of ICP-MS.

LITERATURE CITED

1. Douglas, D. J.; Houk, R. S. Prog. Anal. Atomic Spectrosc., in press 1985.
2. Houk, R. S.; Fassel, V. A.; Svec, H. J. Dynamic Mass Spectrom. 1981, 6, 234.
3. Gray, A. L.; Date, A. R. Analyst 1983, 108, 1033.
4. Douglas, D. J. SCIEX Inc., patent pending 1985.
5. Franklin, J. L.; Studniarz, S. A.; Ghosh, P. K. J. Appl. Phys. 1968, 39, 2052.
6. Seguin, J. G.; Dugan, C. H.; Goodings, J. M. Int. J. Mass Spectrom. Ion Phys. 1972, 9, 203.
7. Rowe, R. Int. J. Mass Spectrom. Ion Phys. 1975, 16, 209.
8. Darcie, T. E. M.Sc. Dissertation, University of Toronto, Toronto, Canada 1979.
9. Darcie, T. E. Institute for Aerospace Studies, University of Toronto, UTIAS Report No. 269 1983.
10. Olson, K. W.; Haas, W. J., Jr.; Fassel, V. A. Anal. Chem. 1977, 49, 632.
11. Douglas, D. J.; French, J. B. Anal. Chem. 1981, 53, 37.
12. Pertel, R. Int. J. Mass Spectrom. Ion Phys. 1975, 16, 39.
13. Trott, G. W.; Beynon, J. H. Int. J. Mass Spectrom. Ion Phys. 1979, 31, 37.

14. Scott, R. H.; Fassel, V. A.; Kniseley, R. N.; Nixon, D. E. Anal. Chem. 1974, 46, 75.

15. French, J. B. Molecular Beams for Rarefied Gasdynamic Research, W. C. Nelson, (Ed.); NATO-AGARD Fluid Dynamics Panel, 1966; AGARD-ograph 12, p. 19.

16. Houk, R. S.; Svec, H. J.; Fassel, V. A. Appl. Spectrosc. 1981, 35, 380.

17. Houk, R. S.; Montaser, A.; Fassel, V. A. Appl. Spectrosc. 1983, 37, 425.

18. Aeschbach, F. Spectrochim. Acta 1982, 37B, 987.

19. Blades, M. W.; Hieftje, G. M. Spectrochim. Acta 1982, 37B, 191.

20. Blades, M. W. Spectrochim. Acta 1982, 37B, 869.

21. De Galan, L. Spectrochim. Acta 1984, 37B, 537.

22. Boumans, P. W. J. M.; De Boer, F. J. Spectrochim. Acta 1977, 32B, 365.

23. Robin, J.; de Lyon, I. ICP Information Newsletter 1979, 4, 495.

24. Fassel, V. A. Science 1978, 202, 183.

25. Fassel; V. A.; Kniseley, R. N. Anal. Chem. 1974, 46, 1110A.

26. Barnes, R. M. CRC Crit. Rev. Anal. Chem. 1978, 7, 203.

27. Olivares, J. A.; Houk, R. S. Int. J. Mass Spectrom. Ion Proc., submitted 1985.

SECTION III.

MATRIX INTERFERENCES ON THE ANALYTICAL SIGNAL OF COBALT BY VARIOUS CONCOMITANT SALTS IN AN INDUCTIVELY COUPLED PLASMA MASS SPECTROMETER

INTRODUCTION

The use of inductively coupled plasma-mass spectrometry (ICP-MS) for elemental analysis is growing with the advent of commercial instruments. Yet, matrix interferences in ICP-MS have been little explored. Such interferences were found to be severe in the early instruments; as little as 100 mg L^{-1} Na was found to cause 10% suppression in the analytical signal of 10 mg L^{-1} cobalt and chromium solutions (1). The sampling orifice used in this early work consisted of a pinhole of < 0.1 mm diameter. Ions were sampled from a thin aerodynamic and electrostatic boundary layer that formed in front of the sampling plate. In order to overcome the adverse effects of this type of sampling (orifice clogging, oxide formation and short orifice lifetime), samplers of large orifice diameter $\gtrsim 0.5$ mm are now used. The higher gas load is handled by an additional pumping stage containing a conical skimmer that skims a portion of the supersonic jet for introduction into the high vacuum region of the mass spectrometer (2-4). This technique is called continuum sampling.

Gray and Date (2) found that their continuum sampler tolerated up to 1000 mg L^{-1} sodium concentrations with only 10% decrease in signal for 10 mg L^{-1} bismuth and cobalt solutions. Douglas et al. (3) also found no interference from phosphate or aluminum concentrations of up to 1000 mg L^{-1} on 2 mg L^{-1} calcium solutions. These authors also reported that trace analysis of chromium, cobalt, copper and manganese in a low

alloy steel (SRM 362) required only calibration with reference standard solutions and no matrix matching was necessary. This was not the case in their determination of nickel, cadmium and copper in NBS water (SRM 1643a) where matrix matched calibration was necessary to assure some accuracy. Furthermore, they only report a qualitative analysis of a marine sediment sample containing approximately 5000 mg L^{-1} dissolved solids.

The extent of these interferences are generally similar to or worse than those found by emission spectroscopy using the ICP (5-9). The actual physical basis for the lower salt tolerance in ICP-MS is still undetermined, but can be attributed partly to salt deposition on the sampling orifice. Some salts are less volatile than others so some condensation on the sampling cone walls may occur since the gas temperature in the sampling orifice is around 3000 K (3).

Several proposed ionization and excitation mechanisms in the ICP have been reviewed recently (10) but little has been established on the mechanism for the dependence of analyte ion signal on salt loadings. Mermet and Robin (11) and Jarosz et al. (12) established a relationship which considers conservation of matter and charge neutrality to calculate densities of neutral atoms, ions and electrons from the Saha equation, under high salt loadings. They verified that local thermodynamic equilibrium is not established in the system, and that the formulation was not generally applicable to the enhancement or suppression of atomic emission signals by the presence of easily ionized elements.

The use of high salt and acid concentrations in ion exchange and solvent extraction methodologies, for which ICP-MS may be used as a multielemental detector, prompted us to investigate the effect of high salt loadings on the observed analytical signal. Thus, in this paper we put aside the fact that the ICP is probably not in local thermodynamic equilibrium and a model with similar ramifications as that shown by Mermet and Robin (11) and Jarosz et al. (12) is presented in order to study the effect of the ionization of different concomitant salts on the analytical signal of a cobalt solution. The salts were chosen so as to contain elements of varying first ionization energies. The calculated trends are then compared to experimental observations using ICP-MS.

THEORETICAL SECTION

Consider the rudimentary ionization reactions possible in the ICP, i.e. the ionization of argon and metal (M) species:

$$Ar \rightleftharpoons Ar^+ + e_o^- \qquad (1)$$

$$M \rightleftharpoons M^+ + e_o^- \qquad (2)$$

which assumes that the analyte M is in low enough concentration that the electron contribution from the ionization of M is negligible compared to the ambient electrons in the ICP, e_o. The equilibrium constants (K) for any such processes are given by Eq. 3,

$$K_i = \frac{n_{i^+}\, n_{e_o}}{n_i} \qquad (3)$$

where n is the number density and the subscripts refer to neutral species (i), ionic species (i^+), or electrons (e_o) in the plasma.

The equilibrium constant can be calculated from the Saha-Eggert equation (13):

$$K_i = 4.84 \times 10^{15}(T_{ion})^{3/2}\ 2\ \frac{Z_{i+}}{Z_i} \exp[-IE/kT_{ion}] \qquad (4)$$

where Z is the partition function, IE the ionization energy (eV) of the element, k is the Boltzmann constant, and T_{ion} is the ionization temperature (K) of the plasma. The ratio of the partition functions can be calculated by the method given by De Galan et al. (14), where T_{ion} is used instead of the excitation temperature. This simplification is valid since the ratio of the partition functions varies very little with temperature in the range 5000-8000 K.

The degree of ionization, α, is defined as

$$\alpha_i = \frac{n_{i+}}{n_{i+} + n_i} = \frac{n_{i+}}{(n_i)_t} \qquad (5)$$

and is derived as a function of the equilibrium constant from equations 3 and 5 to be:

$$\alpha_i = \frac{K_i}{K_i + n_{e_o}} \qquad (6)$$

Now consider the addition, into the ICP, of a salt of composition $A_xB_yC_z$ where the elements, A, B and C may or may not have a relatively

low first ionization energy. As long as enough salt can be added to the ICP there will be some point at which the electron contribution from the concomitant salt will not be negligible and

$$(n_e)_t = n_{e_{Ar}} + n_{e_A} + n_{e_B} + n_{e_C} > n_{e_o} \tag{7}$$

where $n_{e_{Ar}}$ is the contribution of electrons from the ionization of argon in the presence of the interferent. By substituting Eq. 5 and the relationship of the number of molecules of salt $A_xB_yC_z$, Eq. 8 is derived

$$(n_e)_t = \alpha_{Ar} n_{Ar} + n_{ABC}(x\alpha_A + y\alpha_B + z\alpha_C) \tag{8}$$

where n_{ABC} is the number density of molecules of salt injected into the central channel of the ICP. Next, we define γ as the ionization suppression factor of analyte species M due to the presence of salt $A_xB_yC_z$, i.e.,

$$\gamma = \frac{(n_{M^+})_{ABC}}{(n_{M^+})_o} < 1 \tag{9}$$

where $(n_{M^+})_{ABC}$ and $(n_{M^+})_o$ are the analyte ion densities in the presence and absence of the salt $A_xB_yC_z$, respectively. If one assumes that there is no variation in T_{ion} with the introduction of the salt (see Table IV,

Ref. 15) then:

$$(\alpha_M)_{ABC} = \frac{K_M}{K_M + (n_e)_t} \tag{10}$$

From equations 5, 6, 9 and 10 a new expression for γ is derived.

$$\gamma = \frac{K_M + n_{e_o}}{K_M + (n_e)_t} \tag{11}$$

Substituting Eq. 8 for $(n_e)_t$ and rearranging to solve for n_{ABC}:

$$n_{ABC} = \frac{K_M(1-\gamma) + n_{e_o} - \gamma\alpha_{Ar}n_{Ar}}{\gamma(x\alpha_A + y\alpha_B + z\alpha_C)} \tag{12}$$

Assume further that essentially all the electrons in the plasma come from the ionization of Ar when no salt is added. Therefore at $n_{ABC} = 0$, i.e., no interfering salt, $\gamma = 1$ and $n_{e_o} = \alpha_{Ar}n_{Ar} = (K_{Ar}n_{Ar})^{1/2}$. The total number density of particles, n_t, at a particular gas temperature (T_{gas} = 5000 K), and ICP gas pressure (P = 1 atm) is calculated from the ideal gas law:

$$n_t = n_{Ar} + (x + y + z)n_{ABC} = P/kT_{gas} \tag{13}$$

Since for a particular choice of T_{ion} the equilibrium constants are given by Eq. 4, the only unknowns are n_{ABC}, n_{Ar}, α_{Ar}, α_A, α_B and α_C for a particular γ. The α's are each given by an expansion of Eq. 6 with Eq. 8, which are the quadratic equations:

$$\alpha_{Ar}^2 n_{Ar} + \alpha_{Ar}(K_{Ar} + n_{ABC}(x\alpha_A + y\alpha_B + z\alpha_C)) - K_{Ar} = 0 \qquad (14)$$

$$\alpha_A^2 x n_{ABC} + \alpha_A(K_A + \alpha_{Ar} n_{Ar} + n_{ABC}(y\alpha_B + z\alpha_C)) - K_A = 0 \qquad (15)$$

$$\alpha_B^2 y n_{ABC} + \alpha_B(K_B + \alpha_{Ar} n_{Ar} + n_{ABC}(x\alpha_A + z\alpha_C)) - K_B = 0 \qquad (16)$$

$$\alpha_C^2 z n_{ABC} + \alpha_C(K_C + \alpha_{Ar} n_{Ar} + n_{ABC}(x\alpha_A + y\alpha_B)) - K_C = 0 \qquad (17)$$

Therefore, equations 12-17 can be used to solve for the six unknowns at a particular ionization temperature, gas temperature, and various γ values. A reasonable solution to this nonlinear system of equations is achieved using a FORTRAN program using subroutines from the Harwell theoretical subroutine library (16).

For comparison with experimental results it is desirable to relate n_{ABC} to the concentrations of the solution introduced into the nebulizer. This is done using Eq. 19 (12,17) which is derived by substituting the appropriate values into Eq. 18.

$$C_{ABC} = \frac{n_{ABC} F_{AER} T_{gas}}{R_{NEB} E_{NEB} E_{ICP} N_O T_{ROOM}} \tag{18}$$

where: C_{ABC} = concentration of salt in the analyte solution (moles/L)

n_{ABC} = calculated number density of salt injected into the central channel of the ICP (cm^{-3})

R_{NEB} = nebulization efficiency

E_{ICP} = overall transport efficiency of aerosol out of the nebulizer and into the axial channel (estimated to be 75%)

F_{AER} = aerosol gas flow rate (0.5 L/min)

N_0 = Avogadro's number

T_{gas} = gas temperature of axial channel (5000 K)

T_{ROOM} = gas temperature of room (298 K)

For our ultrasonic nebulizer R_{NEB} = 10% and

$$C_{ABC} = 7.4 \times 10^{-17} n_{ABC} \tag{19}$$

The theory presented in this section totally neglects the contribution of the water molecules to the total electron density. Therefore, it is at best a first order approximation to the equilibria existing in the plasma. A more rigorous treatment, that includes the contribution of water, would require the addition of several more equations. Two of these describe the degree of ionization of hydrogen and oxygen. These equations are of the form of Eq. 14 and should present no problem.

The remaining equations must describe the relationship in the change (if any) of water content of the central channel of the ICP with a change in the salt concentration of the analyte solution, along with the dissociation and ionization of H_2O and OH. These are more difficult expressions to derive due to the present limited knowledge about this system.

EXPERIMENTAL SECTION

The ICP-mass spectrometer used for this work is described elsewhere (4). Main ICP parameters were: aerosol gas flow rate 0.4 L/min; outer gas flow rate 17 L/min; auxiliary gas flow rate 0.4 L/min; ICP forward power 1.1 kW; sampling position on center 7 mm above the load coil. The cobalt ion signal in each sample solution was determined with the mass spectrometer set up for single ion monitoring at m/z = 59. Sample solutions were introduced by flow injection to minimize salt deposition and orifice plugging (1). Injections through a 0.5 mL injection loop with a solvent (H_2O) flow rate of 1.7 mL/min to an ultrasonic nebulizer (18) along with desolvation provided eluting peaks with peak heights that were approximately 90% of the signal observed under continuous flow of the analyte into the nebulizer.

Stock solutions of 2.0 M and 0.20 M NaCl, $MgCl_2$, NH_4I, NH_4Br and NH_4Cl were prepared from reagent grade chemicals; $MgCl_2$ stock solutions were prepared from $MgCl_2 \cdot 6H_2O$. Solutions of appropriate molar concentrations of the salts were prepared by diluting the stock solutions and then spiking with a 1000 mg L^{-1} Co standard so as to contain a final Co concentration of 2.0×10^{-5} M (1.2 mg L^{-1}). The Co standard in distilled water was prepared at the same Co concentration.

Each injection of salt solution was preceded and followed by one injection of Co standard in deionized H_2O. Peak heights, with background subtracted, were recorded for each injection. The ratio of the

cobalt ion signal in the presence of a concomitant salt to the average of the cobalt ion signal for the two flanking injections of the cobalt standard was calculated for each salt solution. This corrects for orifice plugging or any change in sampling conditions between injections. At least two trials were performed for each salt. The averages of these ratios were then plotted. The points were connected by straight lines to serve as a visual aid and do not represent a statistical fit to the data.

The mass spectra reported in this paper were recorded with the electron multiplier detector in the analog mode using a current-to-frequency converter (Model No. 151, Analog Technology Co., Pasadena, CA). This insured observation of the major ions in the spectra without the signal losses that occur using ion counting procedures with high ion currents. A mass discrimination correction curve was prepared by recording the complete spectrum of four elements (Na, Co, Y and Pr) at equimolar concentrations. The mass spectra were recorded using a signal averager (Model No. 1170, Nicolet Instrument Co., Madison, WI) for a total of 15 seconds and 128 sweeps, 40 seconds after injection of a 1.0 mL sample. It was critical to collect the mass spectra in the flattest portion of the top of the elution peak, thus assuring the recording of the ion composition sampled from the ICP under the full effect of the salt solution.

The nebulization efficiency of the ultrasonic nebulizer used in this work was estimated by collecting the unnebulized "drain" solution at the nebulizer after uptake of 10 mL of solution to the nebulizer.

RESULTS AND DISCUSSION

In Figure 1, the experimentally measured ratio of cobalt ion signal in the presence of the concomitant salt over the cobalt ion signal from a pure water standard (γ) is plotted versus the salt concentration. The degree of signal attenuation increases with salt concentrations above 0.01 M. This molar concentration corresponds to a total solute level of approximately 0.06-0.15%, depending on the salt, which is in reasonable agreement with maximum total solute levels recommended by other workers (19) for ICP-MS. The amount of salt that can be tolerated at a particular γ increases in the order NaCl < $MgCl_2$ < NH_4I < NH_4Br < NH_4Cl. This trend follows the ionization energies of the most easily ionized element in the salt, i.e., Na < Mg < I < Br < Cl. The curve due to the presence of $MgCl_2$ has a more gradual descent than the others. This is due to apparent clogging of the sampling orifice, presumably due to MgO formed adjacent to the sampling cone. Magnesium oxide has a reported boiling point of 3600 C (20), which is higher than the estimated gas temperature in the sampling orifice and certainly higher than the temperature of the sampling cone walls. This affects the results by causing the signal for a subsequent injection of pure cobalt standard to decrease from its previous value. Even though flow injection and normalization with the results from subsequent injections of Co in deionized H_2O corrects to some extent for orifice plugging and sampling fluctuations, when the

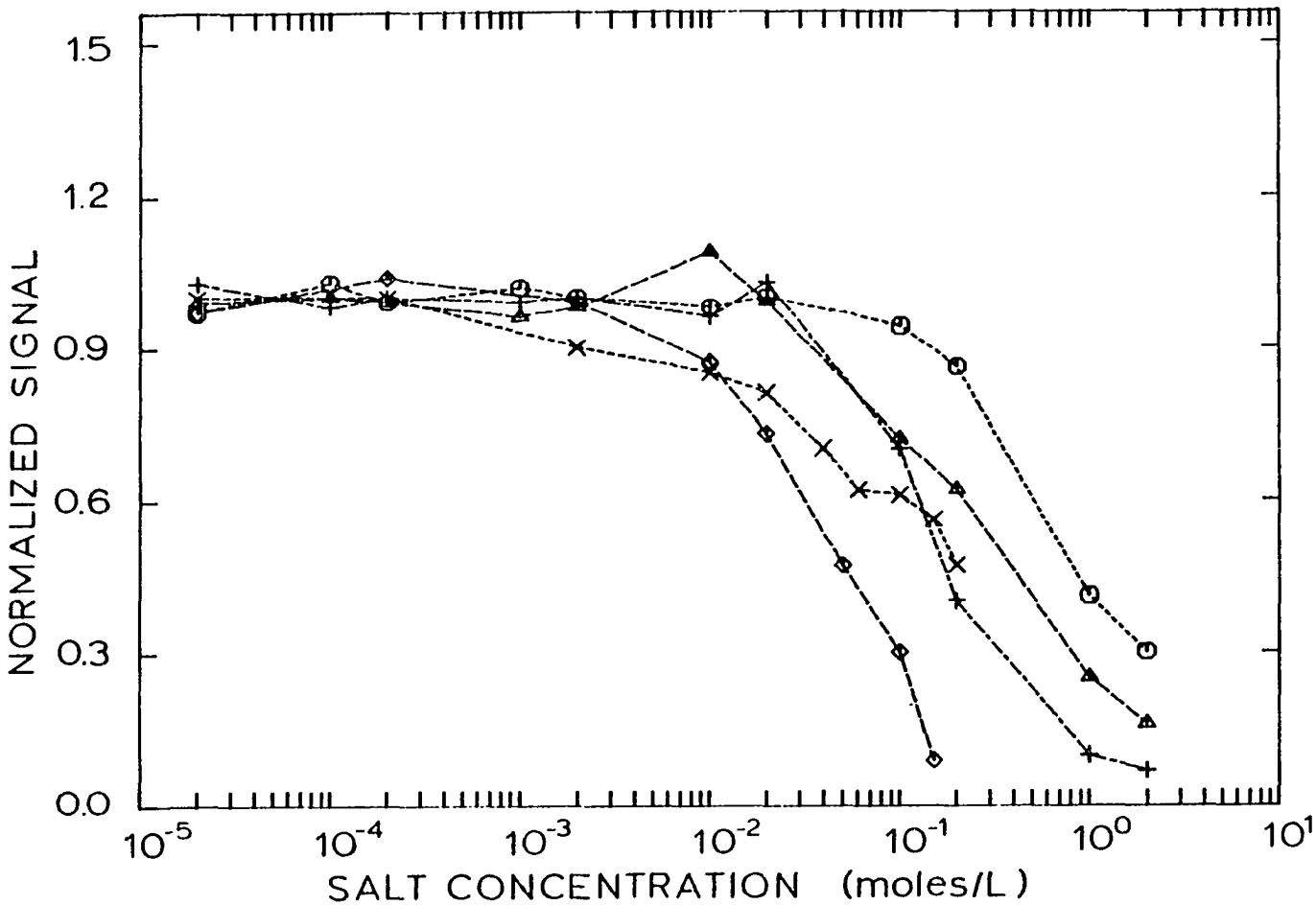

Figure 1. Experimentally determined suppression of cobalt ion signal versus concomitant salt concentration. Matrix salt: (◇) NaCl ; (x) $MgCl_2$; (+) NH_4I; (Δ) NH_4Br; (○) NH_4Cl

problem becomes severe the results become biased at high salt concentrations. This is the case for MgO where the pressure in the first stage dropped from 1.5 to 0.8 Torr after one complete run, i.e., ten injections of salt solution with increasing concentrations.

Solving the equations presented in the theoretical section gives the relationship shown in Figure 2 for the five salts under study and cobalt as the analyte using a typical T_{ion} of 7500 K (21). The overall shape of the theoretical curves and the predicted trends in the extent of signal suppression for the various salts agree with the experimental observations given in Figure 1. The theory predicts greater tolerance to dissolved salts than actually observed. In the case of NaCl, the experimental data show signal suppression at NaCl concentrations one to two orders of magnitude lower than predicted by the theory. Our choice of T_{ion} = 7500 K for the calculations given in Figure 2 is based on the fact that elements with high first ionization energies are extensively ionized in the ICP. For example, iodine has been determined to be 40% ionized (22) in the plasma which at electron number densities of 5 x 10^{14} cm^{-3} (15) corresponds to T_{ion} of approximately 7400 K. The chosen T_{ion} is arbitrary and represents a reasonable value for the ICP. Experimental measurements of T_{ion} vary over several hundred degrees for a particular electron number density (21). Figure 3 shows the relationship between predicted amount of interference with change in NaCl concentration at various values of T_{ion}. The interference effect can

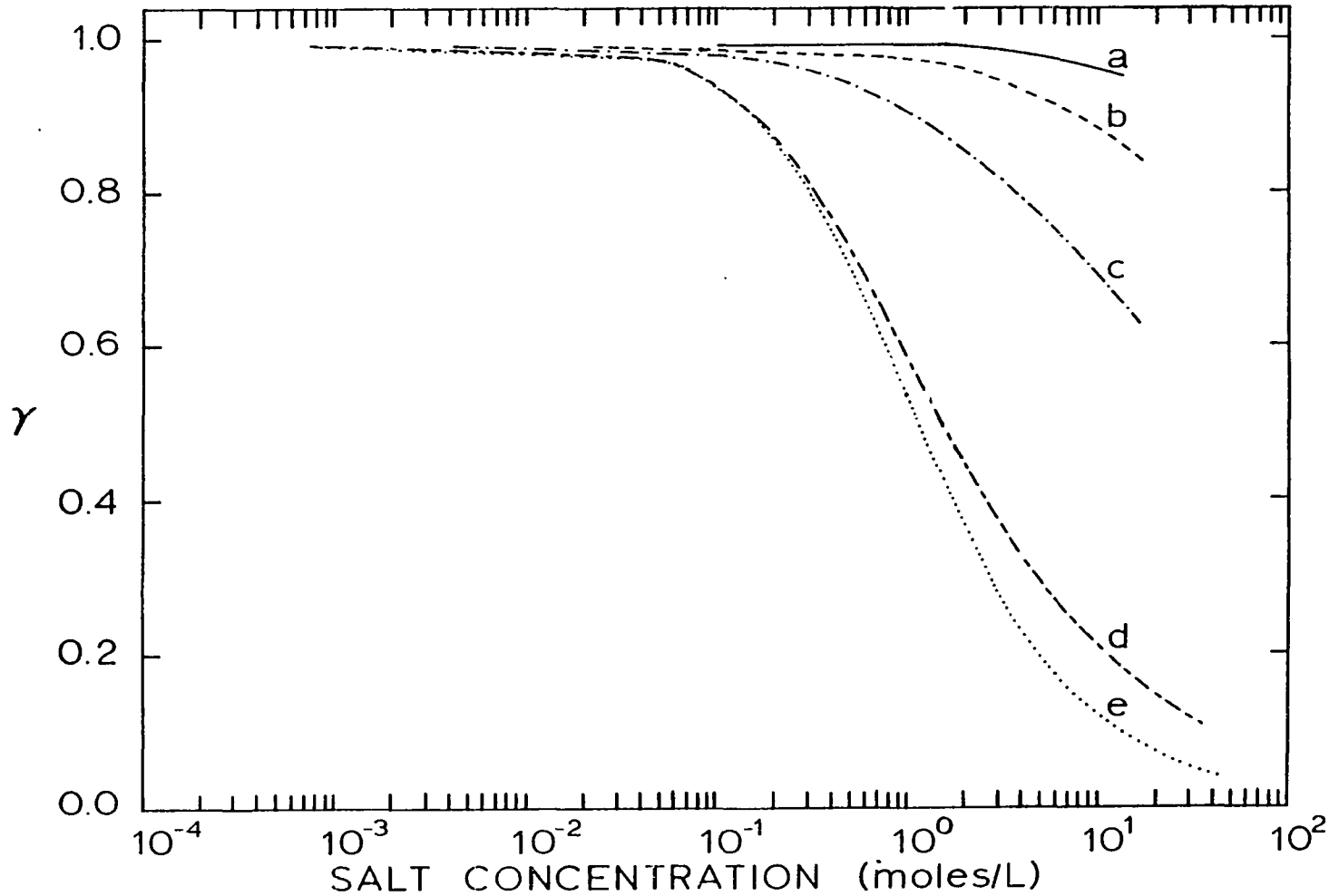

Figure 2. *Theoretically determined suppression of cobalt ion signal versus concomitant salt concentration, at* T_{ion} = 7500 K. Matrix salt: (a) NH_4Cl; (b) NH_4Br; (c) NH_4I; (d) $MgCl_2$; (e) NaCl

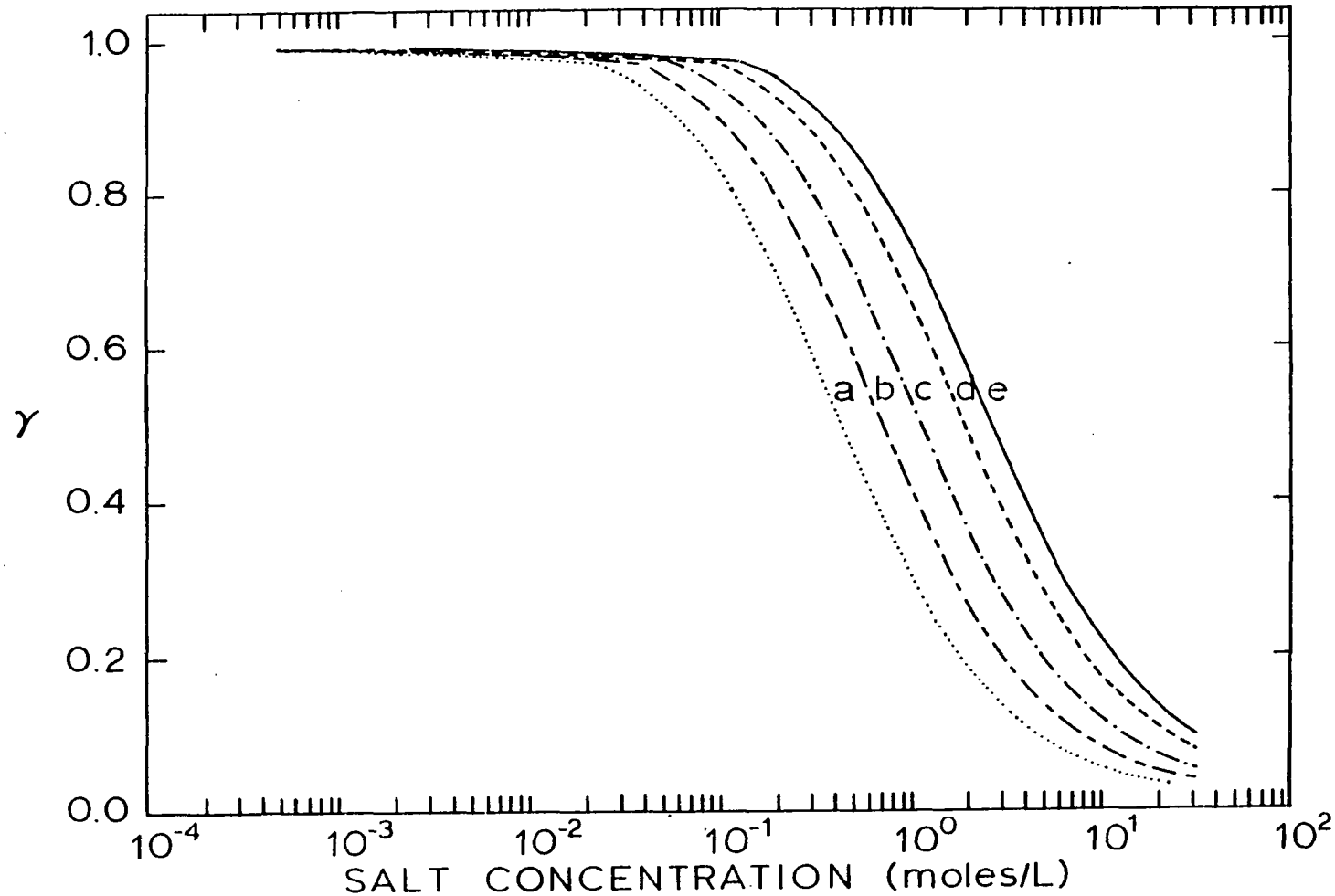

Figure 3. Theoretically determined suppression of cobalt ion signal versus concomitant NaCl concentration at different T_{ion}: (a) 7000 K; (b) 7250 K; (c) 7500 K; (d) 7800 K; (e) 8000 K

vary over one order of magnitude for a change from 7000-8000 K for T_{ion}.

The experimental results shown here for NaCl are approximately one order of magnitude worse than those observed by Bear (9) using the same type of ultrasonic nebulizer and emission spectrometry, and are similar to the results of Date and Gray (2) using a pneumatic nebulizer and mass spectrometry.

Mass Spectra for Concentrated Salt Solutions

The above theory predicts that $(n_e)_t$ will increase at high salt concentrations (Figure 4). In fact such increases should be noticeable even at salt contents of several tenths molar. This relationship should be observable by mass spectrometry. The total ion count rate in the mass spectrum should increase if the total electron number density in the plasma increases because the plasma will remain electrically neutral. An attempt to measure the total ion concentration at several different high salt concentrations (0.02, 0.2, 2 M) was made. The results were erratic and no particular trends in the data could be established. This could be due to sampling problems mentioned in the previous section. However, it was also observed that the capacitor settings on the automatic impedance matching network changed when salt concentrations above 0.2 M were introduced into the ICP, suggesting a significant change in the electrical impedance of the ICP. The capacitor settings returned to normal when the salt solution was spent. Future experiments

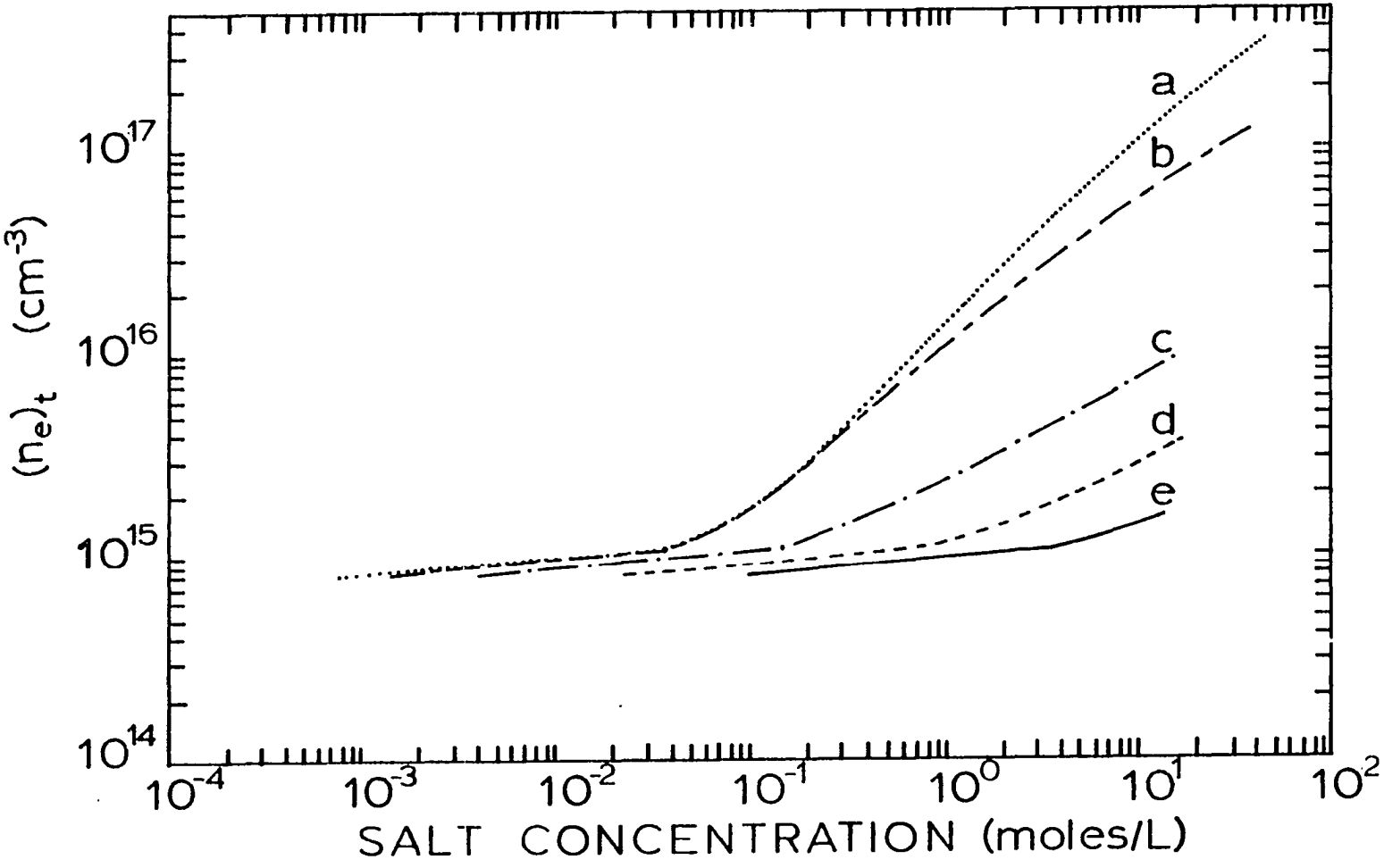

Figure 4. Theoretically determined total electron number densities versus concomitant salt concentration, at T_{ion} = 7500 K. Matrix salt: (a) NaCl; (b) $MgCl_2$; (c) NH_4I; (d) NH_4Br; (e) NH_4Cl

in the measurement of total ion currents will be performed using lower salt concentrations (0 to 0.02 M) in order to avoid the adverse effects of very high salt loadings.

Despite these experimental difficulties there are some interesting qualitative features in the detected mass spectra at high salt concentrations. In particular, the Ar^+ signal tends to decrease as the concentration of injected salt increases (Figures 5-7). Table I summarizes this phenomenon for all five salts. The results in Table I are corrected for mass discrimination. In the last column, a value of 1.00 for the ratio indicates that the argon ion has been completely suppressed. Note that even NH_4Cl suppresses Ar^+ if enough salt is added. Also for 0.2 M NaCl, Na^+ almost totally replaces the Ar^+ signal. The ArH^+, O^+, OH^+ and H_2O^+ peak heights are less dependent than Ar^+ on salt concentration. If these spectra are representative of the ICP (which is hard to evaluate), then, the ionic composition of the central channel of the ICP is made up primarily of Na^+, rather than Ar^+, when a 0.2 M NaCl solution is introduced into the nebulizer. The general trends in Table I are predicted by the theory presented above, not merely because of the constraint of Eq. 13, but also because Eqs. 4 and 6 predict a decrease in the degree of ionization of any element, including argon, with increasing electron number density.

The observation that positive ions from salt constituents can suppress or replace Ar^+ could also be attributed to charge exchange reactions in the ICP:

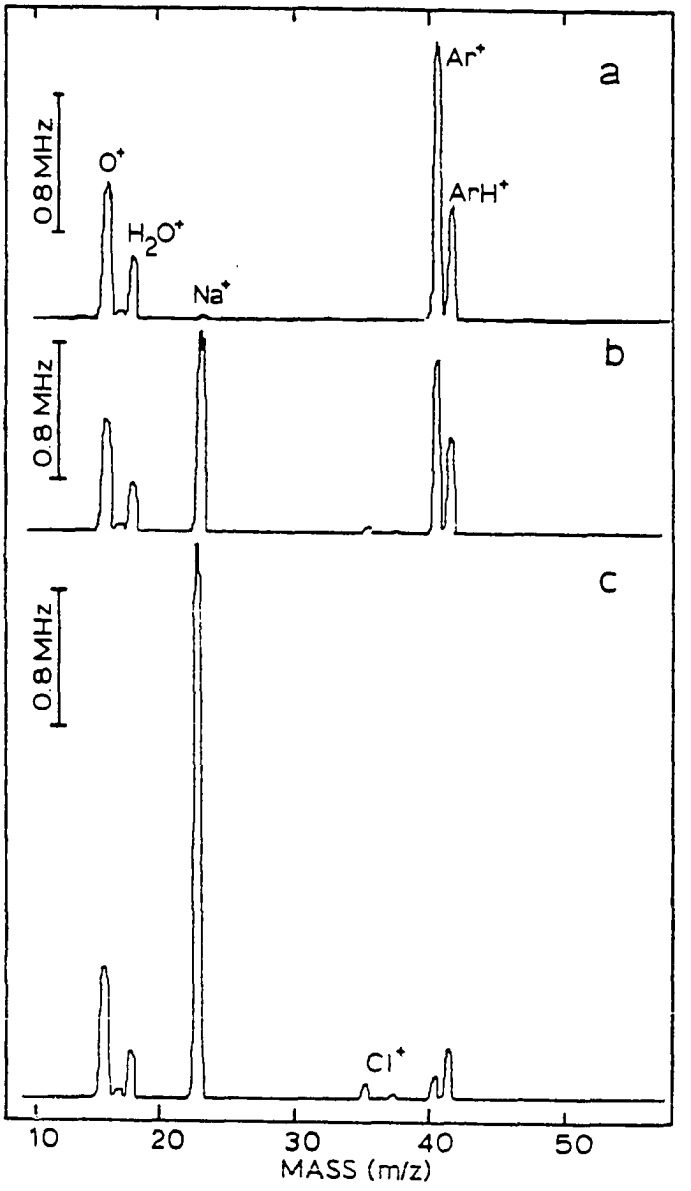

Figure 5. Mass spectra of three solutions of varying NaCl concentration: a) Blank; b) 0.020 M; c) 0.20 M

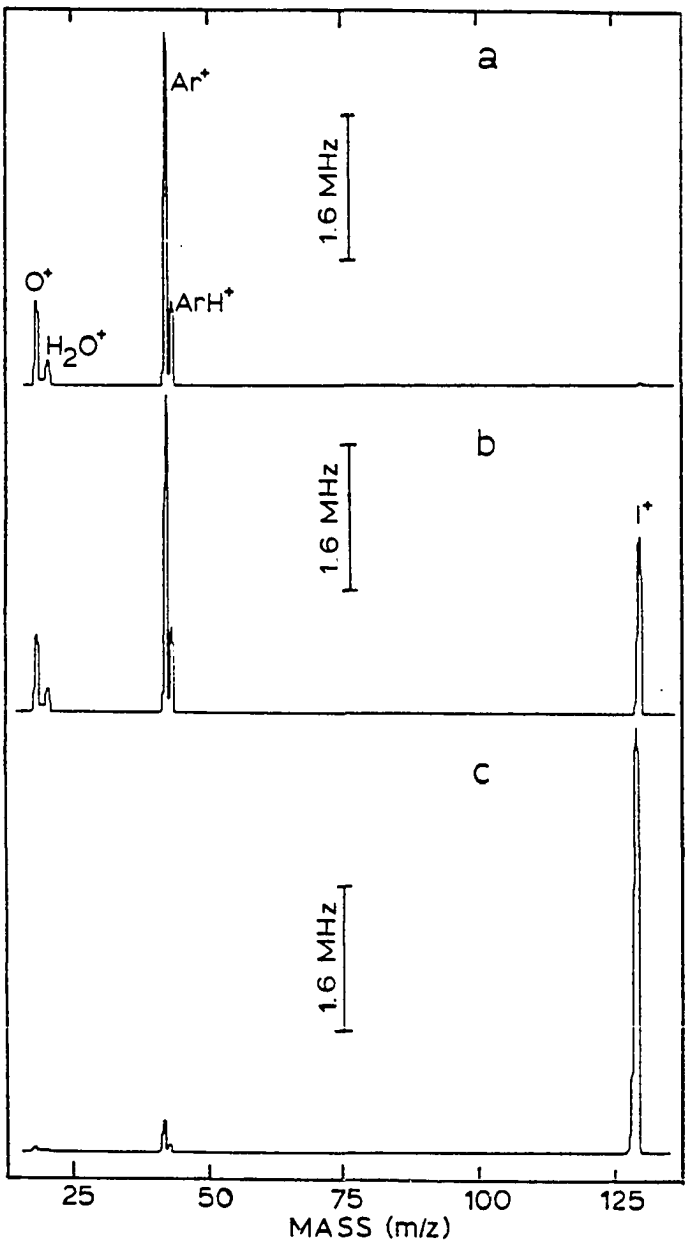

Figure 6. Mass spectra of: a) Blank; b) 0.02 M NH_4I; c) 2.0 M NH_4I

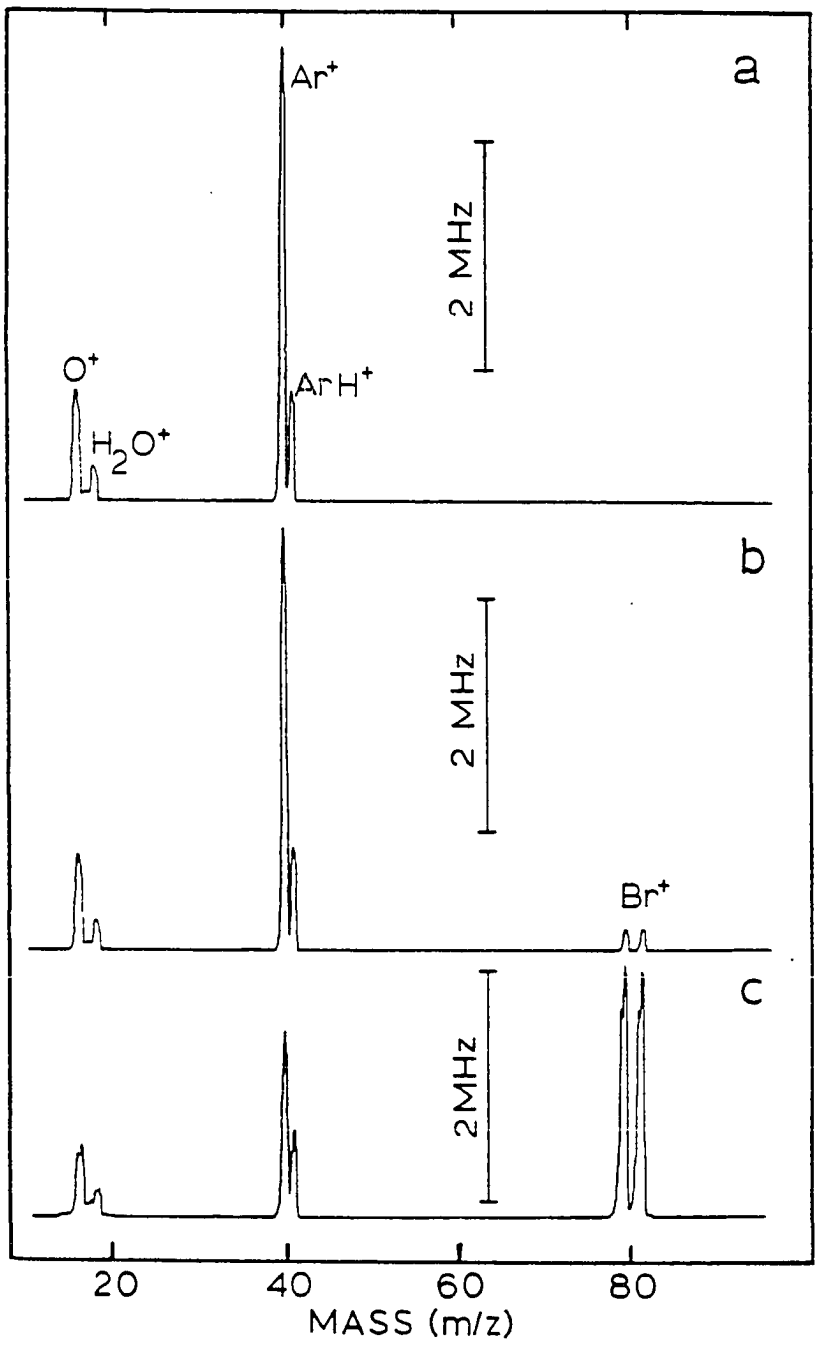

Figure 7. Mass spectra of: a) Blank; b) 0.02 M NH_4Br; c) 2.0 M NH_4Br

Table I. Experimentally Measured Ion Ratios for Five Salts Introduced into the ICP at High Solution Concentrations

Salt	Solution Concentration(M)	Interfering Ion (i^+)	$\frac{Ar^+}{tot^+}$	$\frac{i^+}{tot^+}$	$\frac{i^+}{i^+ + Ar^+}$
Blank	0	none	0.48	0	0
NH_4Cl	0.020	$^{35,37}Cl$	0.44	0.0019	0.0043
	2.0		0.27	0.10	0.27
NH_4Br	0.020	$^{79,81}Br$	0.48	0.012	0.025
	2.0		0.27	0.20	0.42
NH_4I	0.020	^{129}I	0.45	0.029	0.059
	2.0		0.27	0.40	0.60
$MgCl_2$	0.020	$^{24,25,26}Mg$	0.24	0.25	0.51
	0.20		0.012	0.44	0.97
NaCl	0.020	^{23}Na	0.14	0.39	0.74
	0.20		0.011	0.69	0.98

$$Ar^+ + M \rightarrow (M^+)^* + Ar \qquad (20)$$

$$Ar^+ + M \rightarrow M^+ + Ar \qquad (21)$$

where $(M^+)^*$ represents an excited electronic state of the salt ion. These reactions have been proposed to contribute to analyte ionization in the ICP (21,23). Such reactions could be important processes in the plasma due to the large number of collisions possible in this atmospheric pressure source, and should certainly compete with other ionization processes involving collisions between heavy atoms, e.g., Penning ionization (24). However, the present work does not prove the occurrence of charge exchange reactions in the ICP conclusively. In fact, conclusive evidence for this phenomenon versus the ionization suppression effect presented by the above theory can be obtained by ICP-MS only if the measurement of total ion current can be made without bias from salt transport and orifice clogging effects, as are observed in this type of experiment. Basically, if the ionization process in the plasma is due mainly to charge exchange, then the net number density of electrons, and therefore the measured ion current should remain constant even at very high analyte salt concentrations. On the other hand, if ionization suppression by mechanisms that increase the electron density of the ICP as predicted by the theory presented here is dominant, then the electron number density and therefore total ion intensity should increase with increasing salt concentration. The ICP-mass spectrometric approach

provides a potentially attractive means to study this phenomenon because it can directly monitor Ar^+ which does not emit intense enough lines in the visible or ultraviolet regions for study by emission spectroscopy.

Finally, we note several other observations. The nebulization efficiency did not change with solute concentration (Table II) and therefore this did not cause the observed signal suppression. Changing the sampling position to 5, 7 and 9 mm above the load coil caused no discernable change in the Co^+ signal response in a 0.2 M NH_4Cl matrix relative to the pure standard. The ICP-mass spectrometer has a very complex set of operating parameters many of which will certainly affect the observed analytical signal (25). Therefore, a more in-depth spatial profile of such measurements under different parameter settings must be obtained in order to understand this system properly.

Table II. Range of Experimentally Determined Nebulization Efficiency of the Ultrasonic Nebulizer for Three Determinations

Solution	Wt. % Salt	Efficiency (%)
H_2O	0	10.0 - 10.1
2.0 M NaCl	12	9.5 - 10.0
2.0 M NH_4Br	19	9.0 - 10.0
2.0 M NH_4I	29	10.0 - 10.1

CONCLUSION

It is clear from the results and discussion presented that the suppression of analyte signal in ICP-MS in the presence of high concentration matrix salts is partly due to the effect of the ionization of the elements from the concomitant salt and possibly their total contribution to the electron densities in the plasma. The theoretical treatment presented gives the general trend for the suppression of the analytical signal due to the ionization of the concommitant salt, but no effort was made to improve or explain the effects due to aerosol transport efficiency or mass spectrometer sampling conditions. The ICP-mass spectrometer already shows considerable tolerance for high salt concentrations. Further understanding of the limitations observed at present and the theoretical basis for such phenomena should make it possible to predict what chemical systems can be studied directly by ICP-MS without previous sample preparation, e.g., dilution, matrix matching of standards, or chemical removal of matrix elements from samples.

LITERATURE CITED

1. Houk, Robert S.; Fassel, Velmer A.; Flesch, Gerald D.; Svec, Harry J.; Gray, Alan L.; Taylor Charles E. Anal. Chem. 1980, 52, 2283.
2. Date, A. R; Gray, A. L. Analyst 1983, 108, 1033.
3. Douglas, D. J.; Quan, E. S. K; Smith, R. G. Spectrochim. Acta 1983, 38B, 39.
4. Olivares, J. A.; Houk, R. S. submitted to Int. J. Mass Spectrom. Ion Proc. 1985.
5. LaFreniere, K. E.; Rice, G. W.; Fassel, V. A., Ames Laboratory-USDOE and Department of Chemistry, Iowa State University, Ames, IA, manuscript in preparation 1985.
6. Fassel, Velmer A. Science 1978, 202, 183.
7. Larson, George F.; Fassel, Velmer A.; Scott, Robert H.; Kniseley, Richard N. Anal. Chem. 1975, 47, 238.
8. Boumans, P. W. J. M.; DeBoer, F. J. Spectrochim. Acta 1976, 31B, 355.
9. Bear, Bruce R. M.S. Dissertation, Iowa State University, Ames, Iowa, 1983.
10. De Galan, L. Spectrochim. Acta 1984, 39B, 537.
11. Mermet, Jean-Michel; Robin, Jacques Anal. Chim. Acta 1975, 70, 271.

12. Jarosz, Jean; Mermet, Jean-Michel; Robin, Jacques C.R . Acad. Sci. Ser. B 1974, 278, 885.

13. Boumans, P. W. J. "Theory of Spectrochemical Excitation"; Hilger and Watts: London, 1966; Chapter 7.

14. De Galan, L.; Smith, R.; Winefordner, J. D. Spectrochim. Acta 1968, 23B, 521.

15. Kalnicky, D. J.; Fassel, V. A.; Kniseley, R. N. Appl. Spectrosc. 1977, 31, 137.

16. United Kingdom Atomic Energy Authority, HARWELL Subroutine Library, July 1983.

17. Houk, R. S.; Fassel, V. A.; Svec, H. J. "Dynamic Mass Spectrometry" Vol. 6; D. Price and J. F. J. Todd (eds.); Heyden: Philadelphia, 1981; Chapter 19.

18. Olson, K. W.; Haas, W. J., Jr.; Fassel, V. A. Anal. Chem. 1977, 49, 632.

19. Douglas, D. J.; Houk, R. S. Prog. Anal. Atomic Spectrosc., in press, 1985.

20. "CRC Handbook of Chemistry and Physics" 58th Ed.; CRC Press: Ohio, 1977-1978; p. B-128.

21. Houk, R. S.; Svec, H. J.; Fassel, V. A. Appl. Spectrosc. 1981, 35, 380.

22. Houk, R. S.; Olivares, José A. Spectrochim. Acta 1984, 39B, 575.

23. Batal, A.; Mermet, J. M. Can. J. Spectrosc. 1982, 27, 37.

24. Houk, R. S. Report IS-J-918; U.S. Department of Energy, Washington, DC, 1984.

25. Olivares, José A.; Houk, R. S. submitted to Appl. Spectrosc., 1985.

SUMMARY AND THOUGHTS FOR FUTURE RESEARCH

The primary objectives of this thesis have been demonstrated in the preceding sections. It is now possible to design an ICP-mass spectrometer interface in such a manner that its performance can be partly predicted by the physical characteristics of the interface. Yet, there is still much more to uncover about the behavior of this instrument when sampling ions from an ICP. It has been observed that sampling orifice size will contribute to the extent of the pinch discharge formed, and therefore the characteristics of the ions sampled. But no systematic performance studies using various orifice diameters and lengths have been published to date. A knowledge of the above relationship will greatly minimize the uncertainty as to how much pinch the particular design will have, which is of major importance to instrument manufacturers.

Ion focusing and ion detection systems represent more than 50% of the work spent on the ICP-mass spectrometer by the author. But there is little in this thesis that reflects that effort, mainly because existing designs of such systems show the limited knowledge that is available about ion collection and focusing in the transition flow region behind the skimmer. In the future, it should be worthwhile to characterize the flow of ions from the ICP into a vacuum chamber with a supersonic nozzle and skimmer, and to determine the effect of electrostatic fields from simple, one to four lens, systems on such flows. The off-axis detector

arrangement used in this thesis shows that ion detection may best be handled by two different approaches: 1) background suppression, and 2) noise suppression. Clearly, the two are related since a suppression in the background should also lead to a noise suppression due to counting statistics. But, the noise observed on the background signal in our instrument is always higher than that predicted by counting statistics, suggesting a true signal fluctuation due to ion scattering, secondary ionization and electrical noise in the detector. Thus, the background may be minimized by using detectors or detector arrangements that are insensitive to the high photon background from the ICP, e.g., Faraday cup and Daly detector, or ion beam modulation using an electrical chopper. On the other hand additional noise may be minimized by reducing the working pressure in the analyzer and detector chambers to the ultra-high vacuum region. This is commonly done with instruments dedicated for high precision isotopic ratio and elemental analysis, e.g., thermal ionization mass spectrometers, and should be seriously considered for state-of-the-art ICP-mass spectrometers dedicated to this purpose.

Finally, the study of matrix interferences in ICP-MS is still in its infancy. More detailed knowledge of the effect of ICP parameters and interface construction on the observed analytical signal of different elements in the presence of salts at high concentrations is needed. This, coupled with spatial profiles of ion compositions at high salt

loadings should lead to interesting mechanistic proposals for ionization suppression.

The work presented in this thesis should allow the instrumentalist to design an ICP-mass spectrometer with some confidence as to how the particular design will perform. Therefore, this work should serve as more stepping ground for further development. For the analyst, this work should present some understanding of the complexity of ICP-MS. Even though the analytical capabilities of ICP-MS are now outstanding, further development and research should make ICP-MS an even more remarkable tool for elemental and isotopic analysis.

ACKNOWLEDGEMENTS

My deepest gratitude to Dr. Harry J. Svec who, during the first years of my graduate work at Iowa State, cuddled me under his protective arm, introduced me to the field of mass spectrometry, and continued giving me the advice and encouragement, during these years, that I needed to complete this thesis. I thank Dr. Robert S. Houk who has patiently tolerated my stubborn attitude towards my work and the writing of this thesis. I am also deeply indebted to Gerald D. Flesch, who has in the past five years become an endless source of knowledge, technical help, and an amiable confidant. I also wish to thank Joseph J. Thompson and other members of our group who have assisted me in an endless number of projects. The last section of this thesis was developed from fruitful discussions with Margo Palmieri, with whom it has been an honor to collaborate in several projects.

None of this work would have been possible without the skill, help and assistance of machinists Garry Wells, Tom Johnson and Harry Amenson. John Homer, George Holland, and Harold Skank have provided me with numerous lessons on instrumentation, their assistance is gratefully acknowledged. Dr. David E. Eckels taught me much of what I know about programming, and provided the design for the DAC, his assistance has been instrumental to this work.

I am forever indebted to Mrs. Smith C. Dodge who has been an enormous help in many ways throughout my years in college and graduate school. Finally, to my family I am most indebted, especially to my

father who has always been my mentor, and to Phiyen (my wife), Cecilia, Gabriel, and Javier (my children), this thesis is also their achievement.

The assistance of Betty Beymer in the preparation of this document is gratefully acknowledged. Her technical help and patience with the multitude of corrections that were necessary to bring this document to its final format greatly facilitated the writing of this thesis.